NASA Technical Paper 2509

January 1986

Studies of Condensation Effects on Airfoil Testing in the Langley 0.3-Meter Transonic Cryogenic Tunnel

Robert M. Hall

NASA

NASA Technical Paper 2509

1986

Studies of Condensation Effects on Airfoil Testing in the Langley 0.3-Meter Transonic Cryogenic Tunnel

Robert M. Hall

Langley Research Center
Hampton, Virginia

National Aeronautics and Space Administration

Scientific and Technical Information Branch

Summary

The results of condensation studies in the Langley 0.3-Meter Transonic Cryogenic Tunnel (0.3-m TCT) utilizing the NACA 0012-64, NPL 9510, NACA 0012, NASA SC(3)-0712(B), and CAST 10-2/DOA 2 airfoils are summarized as follows: (1) the value of maximum local Mach number over the airfoil $M_{\ell,\max}$ is the most important correlation parameter for the data; (2) both homogeneous nucleation and condensation on preexisting seed particles can occur, depending on the value of $M_{\ell,\max}$; (3) if poor atomization of the liquid nitrogen (LN_2) injected to cool the tunnel occurs, it is possible for unevaporated LN_2 droplets to cause changes in a pressure distribution at total temperatures greater than those corresponding to local saturation; and (4) airfoil drag measurements do not appear to be particularly sensitive to condensation.

It is also shown that an analysis by Sivier correlates well with the present airfoil data. A simple procedure is then documented to predict minimum operating temperatures in the 0.3-m TCT. Because of the ability to test at temperatures below those corresponding to local saturation before the onset of condensation effects, this procedure predicts increases in Reynolds number capability of up to 22 percent and reductions in on-point liquid nitrogen consumption of up to 22 percent, depending on flow conditions.

Introduction

As part of an overall development of transonic cryogenic wind-tunnel technology, NASA has been investigating the onset of condensation effects in nitrogen as a test gas. (See refs. 1 to 6.) Knowing the temperature at which condensation effects occur becomes important because of the impact of condensation on the minimum operating temperature (MOT) of cryogenic tunnels. At some low temperature, either the test gas begins to experience condensation effects or the gas ceases to simulate the nearly ideal-gas behavior of air encountered in flight. As has been reported in references 7, 8, and 9, nitrogen gas will adequately simulate the flow of an ideal diatomic gas except possibly for conditions at or below saturation temperatures for total pressures approaching 9 atm. Consequently, for operating below 9 atm, the onset of condensation effects will be the limiting factor with regard to the MOT and will, in fact, limit the maximum benefits to be gained by operating cryogenically.

These cryogenic benefits increase at an even faster rate as the tunnel operating temperature is lowered. This is illustrated in figure 1 in terms of percent of increase in tunnel Reynolds number capability for each Kelvin drop in total temperature T_t while operating at a constant value of total pressure p_t. Another benefit of operating at lower temperatures is that the amount of liquid nitrogen (LN_2) injected into the tunnel to absorb the heat of the drive fan also decreases. Since the largest portion of operating expenses is in the cost of LN_2, the percent of decrease in LN_2 required for each Kelvin drop in total temperature for operation at a constant value of chord Reynolds number R_c can be significant, as seen in figure 2. (The expressions necessary to calculate the values for figs. 1 and 2 are discussed in the section entitled "Impact of MOT on Maximum Reynolds Number Capability.") Consequently, every Kelvin drop in T_t can be important in terms of either increased Reynolds number capability or reduced operating costs because of the reduction of LN_2 requirements.

If one does not know the circumstances under which condensation actually occurs, then one is forced to avoid any possibility of condensation effects occurring by testing at total temperatures no lower than the total temperature at which saturation first occurs locally over the configuration or airfoil. (Saturation total temperature is defined as that total temperature which, in combination with a value of total pressure, results in static values of pressure and temperature falling on the vapor-pressure curve for nitrogen gas when the flow is expanded to a particular value of Mach number. Local saturation occurs when the flow has been expanded to the maximum value of Mach number over the model and falls on the vapor-pressure curve.) On the other hand, by investigating the onset of condensation effects at total temperatures below local saturation, one can take advantage of whatever additional benefits are possible in terms of increased Reynolds number capability and reduced operating costs.

The amount of possible temperature reduction available can be seen in figure 3, which shows saturation total temperature as a function of total pressure corresponding to values for maximum local, free-stream, and reservoir Mach numbers for a CAST 10-2/DOA 2 airfoil tested at a high angle of attack. (The example could just as well have been for a three-dimensional configuration.) The temperature difference of 14 K or 15 K between saturation total temperatures corresponding to the value of maximum local Mach number of 1.40 and the value of free-stream Mach number of 0.65 can lead to increases in Reynolds number capability and decreases in on-point operating expenses on the order of 20 percent on the basis of figures 1 and 2.

The present report summarizes the onset of condensation as measured during six different studies

involving pressure-instrumented airfoils in the Langley 0.3-Meter Transonic Cryogenic Tunnel (0.3-m TCT). The airfoils tested included a 0.137-m NACA 0012-64, a 0.152-m NPL 9510, a 0.152-m NACA 0012, a 0.152-m NASA SC(3)-0712(B), and 0.152-m and 0.076-m versions of a CAST 10-2/DOA 2. Concurrent with the airfoil pressure measurements, drag rake data were taken for all the airfoils except the NACA 0012-64. The present report will highlight results from all the airfoil studies and summarize the results in such a fashion as to show correlations among the data results themselves, show correlations between the data and theory, and address an hypothesis made by Wagner in reference 10 that drag measurements will be a very sensitive indicator of condensation effects. On the basis of work presented, MOT boundaries for the 0.3-m TCT will be presented in the paper, and the impact of these boundaries on Reynolds number capability will be discussed. Also, comments will address the applicability of the present MOT's to other tunnels. Finally, the MOT's presented will be just as applicable for three-dimensional testing over aircraft configurations as they are for airfoils.

This paper is an outgrowth of reference 11. Additional information has been included concerning goals of the present research, drag sensitivity comparisons, and predicted benefits of operating at temperatures below those corresponding to local saturation over the model.

Symbols

C_p	static pressure coefficient, $\frac{p-p_\infty}{q_\infty}$
C_p^*	static pressure coefficient at $M = 1$ (see fig. 6)
ΔC_p	difference in C_p due to condensation effects
c	airfoil chord, m
c_d	section drag coefficient from wake measurements
M	Mach number
p	pressure, atm (1 atm = 101.325 kPa)
q	dynamic pressure, atm
R	unit Reynolds number, per meter
R_c	chord Reynolds number
T	temperature, K
$\Delta T(M)$	supercooling based on value of M, K
x	linear dimension, m
α	angle of attack, deg
μ	dynamic viscosity, N-sec/m^2

Subscripts:

ℓ,max	conditions at maximum local Mach number over an airfoil
on	conditions at onset of condensation effects
SAT	conditions corresponding to saturation for a given value of Mach number
SIV	onset conditions as predicted by curve fit to Sivier's analysis (see eq. (1))
t	total conditions
∞	free-stream conditions

Abbreviations:

LN_2	liquid nitrogen
MOT	minimum operating temperature
SAT	saturation

Apparatus and Airfoils

Description of the 0.3-m TCT

The 0.3-m TCT (see fig. 4) is a continuous flow, fan-driven tunnel that uses nitrogen as a test gas and is cooled by injecting LN_2 directly into the flow at a position in the diffuser. Coordinating the rate of LN_2 injection and the drive power of the tunnel provides a range of total temperature from about 80 K to 327 K. The tunnel can also be pressurized from 1.2 to 6.0 atm. The tunnel had two different test-section configurations during the time span of the present experiments. The initial test section was octagonal in shape and was used for both airfoil and three-dimensional configuration testing. This test section was used for the tests of the NACA 0012-64 airfoil, and then it was replaced by a test section 0.20 m wide and 0.60 m high. The second test section was more suitable for airfoil testing and was, in fact, used for the remaining airfoils tested. Both tunnel configurations are described in reference 12 and the tunnel instrumentation is described in reference 13.

Description of Drag Rake

The drag rake is a traversing device designed to step, pause, and record total pressure values from the bottom to the top of the wake region behind the airfoil. The total pressure probe used to measure the momentum deficit due to airfoil drag was located on the tunnel centerline in a plane either 0.21 m or

0.26 m downstream from the center of the airfoil turntable. A more detailed description of the rake is given in reference 13.

Description of Airfoils

The NACA 0012-64 airfoil was 0.137 m long and had a total of 21 pressure orifices on the top side; it is described further in reference 2. (Since the presence and magnitude of condensation effects increase with higher values of maximum local Mach number $M_{\ell,\max}$, only upper-surface pressures were analyzed for the onset of condensation effects because of their higher values of $M_{\ell,\max}$.) A detailed description of the 0.152-m NPL-9510 airfoil is given in reference 6. Upper-surface pressures on this airfoil consisted of 32 orifices of various spacing. The NACA 0012 airfoil was also a 0.152-m model instrumented with 32 orifices on the upper surface. A description of its airfoil coordinates can be found in reference 14. The supercritical 0.152-m NASA SC(3)-0712(B) airfoil also had 32 orifices on the upper surface and is described in reference 15. The ordinates for the 0.152-m and 0.076-m versions of the CAST-10/DOA 2 airfoil are described in references 16 and 17. The longer version had 31 orifices in the upper surface whereas the shorter one had 28. The airfoils tested, their class, and their chord are summarized in table I.

Technique in Determining Onset of Condensation Effects

Two methods were used to determine the total pressure p_t and total temperature T_t at which the onset of condensation is first detected for a particular airfoil and a given set of flow conditions, which include free-stream Mach number M_∞, chord Reynolds number R_c, and angle of attack α.

The first and most usual technique was to take pressure data along a p_t and T_t path that was chosen so as to maintain a constant value of R_c while holding M_∞ and α constant. Five examples of constant chord Reynolds number paths are shown in figure 5. Pressure measurements were taken over a range of total temperatures along the paths shown in figure 5 from values above those corresponding to local saturation at the maximum local Mach number $M_{\ell,\max}$ over the airfoil (which is 1.20 for the example given) down to values below the saturation temperature of the free-stream flow. For the chord Reynolds number path of 16×10^6, data were taken at total temperatures as high as 125 K and at various temperature intervals down to a low value of 82 K. The airfoil pressure distribution (see fig. 6 for the condensation-free distribution along the 16×10^6 path) is then analyzed on an orifice-by-orifice basis to determine the total temperature at which condensation effects appeared for the particular orifice.

As a typical example, differences in pressure coefficient from its condensation-free value ΔC_p for an orifice at $x/c = 0.60$ are shown in figure 7 for the same path. A large number of distributions are taken along each path in order to get an accurate value for the onset total temperature $T_{t,\text{on}}$ at which values of ΔC_p begin to depart from its zero, or unperturbed, value. Finally, to determine the onset of condensation effects for the entire airfoil, the total temperatures at which each orifice experienced a departure in its value of pressure coefficient are examined over the entire upper surface of the airfoil before an overall onset temperature is chosen, as shown in figure 8 for the example case. Consequently, determining a single point of condensation onset for an airfoil at given values of R_c, M_∞, and α sometimes involved taking as many as 50 pressure distributions along the path of investigation.

The second method of determining $p_{t,\text{on}}$ and $T_{t,\text{on}}$ corresponding to the onset of condensation effects was to test at a constant value of p_t and to cool T_t down from a value above that corresponding to saturation over the airfoil at its maximum local Mach number $M_{\ell,\max}$. This approach was necessary when high-pressure onset data were needed. For example, in figure 5, the path of constant R_c equal to 38×10^6 starts at values of total pressure close to 5 atm but does not experience condensation onset until a value less than 4 atm is reached. This difference between pressure required to measure condensation-free data above the local saturation temperature and the pressure at onset increases with the value of maximum local Mach number $M_{\ell,\max}$. Consequently, even though the tunnel might be capable of running with p_t as high as 5.0 atm, onset conditions of only 3.5 atm might be measured when using the first method of holding R_c constant. On the other hand, operating at a constant value of p_t permits onset data to be measured at 5.0 atm.

This second method would also be used during tests when run time was limited. The tunnel conditions could generally be changed much more quickly if only T_t was varied instead of both p_t and T_t. This second method, however, made it somewhat more time-consuming to determine onset since some variation in Reynolds number took place over the path of investigation. This variation could result in differences in an orifice pressure coefficient as a function of T_t independent of condensation onset. (The differences in effects due to Reynolds number variation and condensation were usually easy to distinguish and did not degrade data analysis.) No data were taken using this second method during the tests on the NACA

0012-64, NPL 9510, or NASA SC(3)-0712(B) airfoils. Three condensation onset points for the NACA 0012, one for the longer CAST 10-2/DOA 2, and all seven for the shorter CAST 10-2/DOA 2 were taken using the second method.

Types of Nucleation Processes

There are two distinct processes that can occur in cryogenic wind tunnels that lead to the onset of condensation effects. The primary difference between the processes is related to the availability of seed particles. If there are not enough preexisting seed particles, or nuclei, present in the flow to permit condensation, then the gas must form its own seed particles through the formation of liquid droplets or solid crystals and, thus, undergo what is called homogeneous nucleation. If there is a sufficient number of seed particles already present in the flow, then condensation can occur directly on these seeds without having to wait for the formation of seed particles out of the gas itself. This second process is called heterogeneous nucleation, in which the prefix "hetero" refers to the mixture of gas molecules and the preexisting seed particles for the present case of nitrogen-gas cryogenic tunnels.

As addressed in references 18 and 19, homogeneous nucleation can be predicted by classical liquid droplet theory. One such theoretical investigation of the onset of condensation effects due to homogeneous nucleation in nitrogen was reported by Sivier in reference 20 and is summarized in figure 9. This figure shows the results of Sivier's computer study in which he predicted the onset of condensation effects in a one-dimensional nozzle for a variety of different nozzle expansion rates and for a variety of different total conditions. For the various conditions simulated, the onset of effects, which were defined by Sivier in reference 20 to occur when p reached 1.01 times its condensation-free value, was found to take place within the two curves of figure 9 to the left of the nitrogen vapor-pressure curve. It can be seen in the figure that the allowable range in temperature below the vapor-pressure curve at a given value of pressure depends more on the value of pressure than on the variety of expansion rates and total conditions simulated by Sivier.

The applicability of Sivier's analysis to transonic cryogenic tunnels can be questioned on two grounds. First, the experimental data used for comparison by Sivier were taken in hypersonic tunnels, where the static values of p at onset were 0.01 atm or less. In the case of the Langley 0.3-m TCT or the National Transonic Facility (NTF) at the Langley Research Center, however, p at onset may be on the order of 1 atm. With the sensitivity of onset to the value of p at onset, Sivier's analysis should be checked at the higher pressures of current interest. Second, Sivier's analysis contains some assumptions that are questionable. For example, he assumes for his analysis that the condensate is always in the liquid phase even though onset temperatures during the flow expansions could be 30 K below the triple point. Also, he assumes that the temperature of the liquid drop is at saturation temperature T_{SAT}, independent of droplet radius. Having droplet temperature independent of droplet radius is contrary to most approaches, as typified by reference 19 where critical-sized droplets are assumed to be at gas temperature. Temperature differences between T_{SAT} and T can have an important impact on nucleation rate through the dependence of surface tension on temperature.

Even though the applicability of Sivier's analysis can be questioned, the following curve fit to his onset band

$$\frac{1}{T_{SIV}} = 0.01461 - 0.004962 \log_{10} p + 0.0001959(\log_{10} p)^2 \qquad (1)$$

where T_{SIV} is the predicted onset static temperature for a given value of static pressure p in atmospheres, was found in reference 3 to be consistent with earlier comparisons of the NACA 0012-64 airfoil pressure data and with some flow visualization results taken with the NPL 9510 airfoil. Whether equation (1) can be useful in general for predicting the onset will be examined later in the section "Results and Discussion."

To complement Sivier's analysis, a computer program predicting homogeneous nucleation with provisions for simulating the presence of seed particles has been developed at Langley by Dotson and this author. This program is described in reference 21 and will also be used to analyze the airfoil data.

Heterogeneous nucleation is simply the growth of condensate on preexisting seed particles for nitrogen-gas cryogenic wind tunnels and is relatively easy to model. The problem is in determining the size and number density of the preexisting seed particles. As concluded in reference 5, the best estimate for the seed particles is that they are approximately 0.25 μm in radius and have a concentration of about 3×10^{12} per kilogram of the test gas. These numbers are somewhat uncertain, and further experiments should be planned to better define the preexisting seed-particle population. Until these numbers are substantiated, however, it is necessary to rely on the available experimental data base for predicting MOT because of the uncertainty in size and number density of the seed distribution.

Thus far only homogeneous nucleation of one kind of gas has been considered concerning the formation of condensate. There is another type of nucleation, called "binary nucleation," that occurs when two gaseous species interactively condense. For the present case, however, binary nucleation does not appear to be a possibility during the present experiments because of the high level of purity of the liquid nitrogen that evaporates and forms the test gas. Analysis of two gaseous samples taken from the tunnel during normal operation showed the following concentrations of contaminants:

Contaminant	Sample 1	Sample 2
O_2 (including argon), ppm	350	300
CO, ppm	< 0.1	< 0.1
CO_2, ppm	< 0.1	< 0.1
H_2O, ppm	0.3	0.3
Total hydrocarbons, ppm	< 0.1	< 0.1
Oils, mg/L . . .	< 0.0001	< 0.0001

As can be found in reference 22, these levels of impurities are far below those levels that impacted the onset of condensation in nitrogen gas during the early studies at the California Institute of Technology involving the influence of impurities on the onset of condensation for nitrogen gas.

Results and Discussion

Trends Within the Experimental Data Base

As pointed out in the discussion on determining onset conditions, many pressure distributions had to be examined to determine the 57 condensation onset points reported herein. In fact, the current data summary is based on 1660 pressure distribution measurements that were taken over an 8-year period. In presenting the onset conditions, the data will usually be in a format of supercooling at onset as a function of either maximum local Mach number $M_{\ell,\max}$ or free-stream Mach number M_∞. Supercooling at a given value of Mach number is defined as

$$\Delta T(M) = T_{\mathrm{SAT}} - T_{\mathrm{on}}(M) \qquad (2)$$

where T_{SAT} is the temperature at which the expansion isentrope crosses the vapor-pressure curve and T_{on} is the value of static temperature at onset. To determine supercooling at the point of maximum local Mach number, for example, T_{on} is calculated along the isentrope at a Mach number value equal to $M_{\ell,\max}$. (If the flow were to contain shock waves before the onset of condensation, then T_{on} could be evaluated by using the adiabatic flow equations.)

Figures 10 and 11 highlight the dependence of $\Delta T(M_{\ell,\max})$ on the value of $M_{\ell,\max}$. The first trend to notice in figure 10 is that $\Delta T(M_{\ell,\max})$ is nearly linear with $M_{\ell,\max}$ and that the values of supercooling collapse to within an 8 K band. The second trend is that the data from the different tests, which included six airfoils tested with various values of M_∞ from 0.40 up to 0.95 at angles of attack from 0° to 10°, fall in what appears to be a random fashion over this 8 K band. Consequently, the specific shape of the pressure distribution does not seem to be as important as the value of $M_{\ell,\max}$. Figure 11, which involves only the data from the 0.152-m and 0.076-m CAST 10-2/DOA 2 airfoil tests, shows some minor differences in values of supercooling between the two different lengths; nevertheless, length effects do not appear to be as important as $M_{\ell,\max}$.

More insight can be gained, for example, by examining the amount of supercooling based on free-stream conditions $\Delta T(M_\infty)$ as a function of $M_{\ell,\max}$, which is presented in figure 12. Apart from two low data points at values of $M_{\ell,\max}$ of 0.50 and 0.60, the values of $\Delta T(M_\infty)$ are seen to be relatively constant up to values of $M_{\ell,\max}$ greater than 1.20. Above values of 1.20, a very rapid change occurs in $\Delta T(M_\infty)$ in the negative direction, which corresponds to condensation onset occurring at temperatures above the saturation temperature for M_∞. Consequently, it would seem that condensation onset is actually correlating with free-stream conditions up to a value of $M_{\ell,\max}$ of about 1.20, and then onset begins to occur at temperatures warmer than those corresponding to saturation in the test section. This break in $\Delta T(M_\infty)$ signifies a change in the process from one involving condensate growth upstream of the model on preexisting seed particles to one involving condensation effects occurring locally over the airfoil. The observation in figure 10 that $\Delta T(M_{\ell,\max})$ versus $M_{\ell,\max}$ appears to be linear below values of $M_{\ell,\max}$ of 1.20 is explained by figure 13, which shows that for this particular test program there is a nearly linear relationship between $M_{\ell,\max}$ and M_∞ for values of $M_{\ell,\max}$ less than 1.20.

The last item of interest about the onset data in figure 12 is that at the very low values of $M_{\ell,\max}$ corresponding to 0.50 and 0.60, which resulted from data with M_∞ equal to 0.40 or 0.50, three of the five data points showed values of $\Delta T(M_\infty)$ at onset averaging 0 to 1 K; but two data points displayed values of $\Delta T(M_\infty)$ equal to -7 K or -8 K, which correspond to values of onset appreciably above the corresponding free-stream saturation temperatures.

This situation appears to result from the following circumstance. At the low power requirements resulting from low values of M_∞ combined with relatively low values of tunnel operating pressure, the flow rate of injected LN_2 required for keeping the tunnel cool may be insufficient for efficient atomization to occur at the injection nozzles. (Note: Since these data were taken, the operating system of the 0.3-m TCT has been modified to permit closure of up to three of the four injectors. This operating flexibility should help to eliminate inefficient atomization for future tests.)

Inefficient atomization results in larger LN_2 droplets and, consequently, may result in unevaporated LN_2 reaching the test section and triggering effects in the data. This explanation is consistent with a closer examination of the five data points, which reveals that the two points showing early effects both had values of M_∞ equal to 0.40 (the lowest value tested) and were from tests conducted at low values of tunnel p_t. As an example, the NACA 0012 airfoil data point with $\Delta T(M_\infty)$ equal to 0 at $M_{\ell,\max}$ equal to 0.50 corresponds to identical values of M_∞ and α as the NACA 0012 airfoil data point for which $\Delta T(M_\infty)$ is -8 K, except that p_t is 4.27 atm instead of 1.73 atm. Since tunnel operating power and the amount of LN_2 needed for cooling are proportional to operating pressure, it appears that, indeed, the lower power condition resulted in relatively warmer temperatures at onset.

Relative Sensitivity of Drag Measurements

After making a two-dimensional airfoil calculation for saturated equilibrium condensation in reference 10, Wagner concluded that pressure drag should be very sensitive to the presence of condensation. In concluding his section on equilibrium condensation about airfoils, Wagner remarks that "from the viewpoint of accurate drag prediction only small penetrations are allowed into the condensation region with the restriction that the local Mach number may not . . . exceed the saturation Mach number by more than about 0.1." To examine this prediction of Wagner, a comparison between Wagner's work and the present data can be made. Since Wagner's statement concerning drag was based on the integration of surface pressures calculated from a two-dimensional airfoil code, drag comparisons with the present data can be drawn from either integration of measured surface pressure data or from an integration of the momentum deficit as determined from drag rake total pressure measurements. For subsonic flow, the drag rake measurements are preferred because of better accuracy and because they also would reflect any possible influences of condensation on the airfoil skin-friction losses, which would not show up in plots of pressure drag. As will be seen when comparing the drag rake measurements with integrated surface pressures, the drag rake measurements are, in fact, the more sensitive of the two to the presence of condensation.

One of Wagner's two condensation calculation examples was for flow about an NACA 0012 airfoil with $M_\infty = 0.80$, $M_{\ell,\max} = 1.30$, and $\alpha = 0.37°$. The most similar experimental data taken during the present experimental program were for the NACA 0012 at $M_\infty = 0.76$, $M_{\ell,\max} = 1.28$, $\alpha = 2.0°$, and $R_c = 45.3 \times 10^6$. The experimental values of drag as measured with the rake are shown in figure 14 as a function of both total temperature and saturation Mach number. As can be seen in the figure, although there is scatter in the data, there are no systematic effects for temperatures as low as those at which the data were taken. The drag data can then be cast in Wagner's format (used in fig. 31 of ref. 10) and be compared with his predicted drag increase for his conditions. (See fig. 15.) The flagged data points in figure 15 represent decreases in measured drag, not increases as predicted by Wagner's calculations that are shown by the solid line. For the present data, the local Mach number of 1.28 exceeded the lowest value of saturation Mach number of 0.83 by 0.45 without any systematic effects occurring.

The next closest data run was for the NACA 0012 airfoil with $M_\infty = 0.65$, $M_{\ell,\max} = 1.23$, $\alpha = 4.5°$, and $R_c = 41.1 \times 10^6$. These drag rake data are shown in figure 16 and once again demonstrate the ability to penetrate far below local saturation Mach number before any condensation effects begin. In this second case, the value of M_{SAT} of 0.60 at which onset occurred was below the local saturation Mach number of 1.23 by over 0.6 instead of the value of 0.1 suggested by Wagner. (It should be noted that the onset of condensation effects based on this drag rake data occurs at 96.5 K, as shown in figure 16. The corresponding onset value determined by the usual procedure of an orifice-by-orifice pressure inspection was at 97.5 K.)

For the data at $M_\infty = 0.65$, actual integrated surface pressure drag is shown in figure 17. As can be seen by comparing figures 16 and 17, the integrated surface pressure drag is not nearly as sensitive as the drag rake data; this finding reinforces the present observation that drag is not as sensitive to condensation as was predicted by Wagner. (The difference in absolute magnitude of drag between the surface pressures and drag rake is attributed to the surface pressure orifices not being adequately spaced in a direction normal to the plane of the wing and to the resulting inaccuracies in the integration.)

One possible explanation for the disagreement between Wagner's calculations and the present data may rest with the use by Wagner of the saturated equilibrium expansion model. In particular, an inherent part of the model is the equilibrium model for sound speed which, as described in reference 18, results in a discontinuous drop in sound speed of 20 to 30 percent when passing from unsaturated to saturated flow. This drop in sound speed will manifest itself as higher local Mach numbers over the airfoil and should result in larger wave drag values because of the higher Mach number at the shock location. The increase in wave drag may be responsible for the calculated increase in drag. In any case, this author has not found experimental drag data to be any more sensitive to condensation than the usual orifice-by-orifice examination of the surface pressures.

Correlations Between Data and Theory

Studies utilizing the in-house computer program described in reference 21 for predicting condensation onset due to homogeneous nucleation have confirmed several of the experimental observations. For example, the program has verified the minimal sensitivity of homogeneous nucleation onset to the shape of the pressure distribution as long as the respective values of $M_{\ell,\max}$ are the same. To demonstrate this, three hypothetical pressure distributions were chosen and are shown in figure 18. The distribution labeled "Baseline" was chosen as a close representative of the supersonic flow region of the 0.152-m CAST 10-2/DOA 2 airfoil at an angle of attack of 6° and for a value of M_∞ equal to 0.65. The distribution labeled "Flattop" was chosen to maximize the distance for which the flow was at the maximum value of local Mach number $M_{\ell,\max}$, and the distribution labeled "Spike" was chosen to minimize the distance at $M_{\ell,\max}$.

To compare the condensation growth due to homogeneous nucleation over each of the hypothetical airfoils, the position $x = 0.039$ m was used for a quantitative comparison of the predicted differences in C_p. The differences in pressure coefficient due to condensation ΔC_p as a function of T_t are shown in figure 19 for each of the three distributions. Both of the extreme distributions, Spike and Flattop, result in values of total temperature onset within a 1.0 K band of the Baseline distribution. This 1.0 K band would be undetectable in the overall level of scatter in the current condensation data base and would explain the apparent insensitivity of the data to pressure distribution, as mentioned in the discussion concerning figure 10. (Note: In this report, differences in both supercooling and total temperature at onset are used to describe the data. In general, supercooling differences for the same two data points will be nearly 1.5 to 2.0 times as large as the corresponding differences in total temperature.)

The computer program (ref. 21) was also used to quantify the effects of chord change for similar pressure distributions. With the Baseline distribution of figure 18 and for a hypothetical airfoil 10 times shorter and another 10 times longer than the Baseline airfoil, it is shown in figure 20 that the factors of 10 will only influence the onset total temperature (as determined by a fixed value of ΔC_p) by less than 2.0 K. Consequently, for a difference in chord of only a factor of 2, theory would predict differences in total temperature at onset of less than 0.5 K. Since the differences in supercooling, as shown in figure 11, between the 0.152-m and 0.076-m CAST 10-2/DOA 2 airfoils are within the general level of testing scatter, it is difficult to say whether the calculation exactly matches the data. However, the trends of the data and theory are the same for the onset of condensation due to homogeneous nucleation—increasing the length scale of the experiment results in only mild increases in onset total temperatures.

As mentioned previously, Sivier (ref. 20) completed a computer study predicting the onset of condensation due to homogeneous nucleation in nitrogen gas, and the present author has correlated Sivier's onset-of-effects band in the region of interest to cryogenic tunnels. (See eq. (1).) To examine how well this curve fit to Sivier's results compares with the onset data for the six airfoils, one can look at differences between the value of static temperature at onset T_{on} and the value predicted by Sivier T_{SIV}. For these comparisons, T_{on} is calculated from the experimentally measured onset values of p_t and T_t by assuming that the flow undergoes an isentropic expansion to a Mach number of $M_{\ell,\max}$.

This difference between T_{on} and T_{SIV} is plotted in figure 21 and shows an apparent relationship between the plotted temperature differences and $M_{\ell,\max}$. At the lower values of $M_{\ell,\max}$, the onset temperature is occurring at higher temperatures than those predicted by the curve fit to the Sivier analysis. Since Sivier's analysis is intended to model homogeneous nucleation, either another process—heterogeneous nucleation—is taking place or the analysis is in error. However, as was seen in figure 12 at these lower values of $M_{\ell,\max}$, onset indeed correlates with free-stream conditions and appears to result from growth on preexisting seed particles. Furthermore, the differences between experiment and theory appear to approach 0 as the value of $M_{\ell,\max}$ reaches 1.20 or above. This result is to be expected because as $M_{\ell,\max}$ increases, the local values of p and

T can get farther below the vapor-pressure curve, which strongly increases the rate of homogeneous nucleation and, therefore, the likelihood of homogeneous nucleation influencing the data. Consequently, in cases where Sivier's analysis should apply, there is good agreement.

Whether homogeneous nucleation will be the cause of condensation effects will also depend on the magnitude of M_∞. The lower that M_∞ is in magnitude below $M_{\ell,\max}$, the lower the temperature at which the tunnel can be operated before condensation growth in the test section itself causes heterogeneous effects over the airfoil. Thus, it will be more likely that p and T can get far enough below the vapor-pressure curve to trigger homogeneous nucleation effects. For example, if $M_{\ell,\max} = 1.20$ and $M_\infty = 1.10$ in one case and 0.50 in a second case, then it is much more likely that homogeneous nucleation will occur for the second case where $M_\infty = 0.50$ because the total temperature at which saturation occurs for $M_\infty = 0.50$ is about 9 K lower than that for $M_\infty = 1.10$. This interplay between $M_{\ell,\max}$ and M_∞ can be seen in figure 22, which presents the same data for $T_{\text{on}} - T_{\text{SIV}}$ as a function of $M_{\ell,\max} - M_\infty$. As expected, it can be seen in this format that the curve fit to Sivier's homogeneous nucleation results gives a better prediction of the results in the 0.3-m TCT when the difference between local and free-stream Mach numbers is larger.

An additional direct comparison between the curve fit to Sivier's analysis and the airfoil data base can be made by plotting the data along with the predicted value of total pressure at onset as a function of total temperature by using equation (1) in conjunction with the isentropic flow equations. For example, the solid-line curves in figure 23 represent the predicted operating total pressures at which the onset of condensation effects would occur for the respective maximum local Mach number values of 1.20, 1.30, 1.40, and 1.70 compared with airfoil data for which $M_{\ell,\max}$ was within ± 0.03 of the respective value. Flagged data symbols signify that the airfoil onset occurred below free-stream saturation temperature. (For the flagged symbols, consequently, it is uncertain as to whether onset was the result of homogeneous nucleation, in which case equation (1) should apply, or the result of condensate growth on preexisting seed particles upstream of the model in the free-stream flow.)

Figure 23(a) compares the curve fit to Sivier's analysis with the experimental data for $M_{\ell,\max} = 1.20$ and shows the onset data generally occurring at values of T_t from 1 K to 4 K higher than predicted. However, all except one of the data points experienced onset below free-stream saturation temperature, so the relatively poor agreement between theory and experimental data may be due to the occurrence of heterogeneous nucleation. Figure 23(b) compares the curve fit and the data for a value of $M_{\ell,\max}$ equal to 1.30. Here the agreement is much better, although the data still seem to have a level of scatter equal to 3 K about the line. Next, figure 23(c) compares the curve fit and the data for a value of $M_{\ell,\max}$ equal to 1.40. Here, the agreement is best and the magnitude of scatter in the data is least. Finally, figure 23(d) compares similar information for $M_{\ell,\max}$ equal to 1.70 and shows values for scatter of about 2 K.

In summary, the curve fit to Sivier's predicted onset of effects does a very satisfactory job of predicting the onset of condensation to within ± 3 K in the 0.3-m TCT data, which is close to the experimental accuracy of the overall test program. In fact, the curve fit to Sivier's analysis gives a prediction of condensation onset as good as that of the computer program described in reference 21. Consequently, because of its simplicity, the curve fit will be used for the condensation calculations to follow.

Prediction of Minimum Operating Temperatures for the 0.3-m TCT

In specifying minimum operating temperatures (MOT's) for general cryogenic testing, the goal of avoiding condensation effects in the test data must be kept foremost in mind. This goal is different from specifying the temperatures at which condensation is most likely to be detected. In the present case, it is necessary to have very conservative boundaries that avoid any reasonable possibility of onset occurring; whereas in the second circumstance, one would use an expression approximating the mean of the experimental values for the occurrence of condensation. Consequently, for the present need of specifying MOT's that avoid condensation effects, a buffer that is larger than the scatter in the data will have to be added to the curve fit to Sivier's analysis. Similarly, a buffer will also have to be added to the tunnel temperatures corresponding to free-stream saturation. Finally, special consideration is also given to tunnel conditions at low power conditions.

The first, and most important, step in prescribing a MOT boundary is to decide what value of $M_{\ell,\max}$ will be expected during the experiment so that the curve fit to Sivier's analysis can be used to predict the total temperatures at which the onset of homogeneous nucleation will occur. If the

value of $M_{\ell,\max}$ is not known beforehand, then a value that tends toward the high side must be estimated. For values of p_t in the range of the experiment, values of p are calculated that occur when the flow has accelerated to $M_{\ell,\max}$. (The ideal-gas equations are accurate enough for the present analysis.) Next, equation (1) is used to determine the corresponding values of static temperature at which the onset of condensation effects would be predicted. Now that values of p_{on} and T_{on} are predicted, the corresponding values of $T_{t,SIV}$ for the various values of p_t can be calculated by again using the isentropic flow equations to go from static back to total conditions. Once $T_{t,SIV}$ is known, a 4 K increment is added to this total temperature as a buffer. For experiments with expected values of $M_{\ell,\max}$ greater than 1.20, this first step will be the most crucial in predicting the MOT boundary because of the predominance of homogeneous nucleation for cases of high local Mach number.

The second step in prescribing a MOT boundary is to make sure that the flow conditions in the free stream are above saturation by an appropriate buffer increment. Again, a value of p_t is chosen and a value of p appropriate for an expansion to M_∞ is then calculated. Now, instead of using the curve fit, one of the following two expressions for the vapor-pressure curve of nitrogen can be used to find the saturated static temperature T_{SAT} for the given value of p in atmospheres. The following equation, taken from reference 23, is used to relate saturation pressure and temperature if the temperature is above the triple point temperature, which for nitrogen is 63.148 K:

$$\log_{10} p = 3.93352 - \frac{304.494}{T_{SAT}} \qquad (3)$$

If the temperature is below the triple point, then the following equation (see ref. 24) describing the vapor-pressure curve is used:

$$\log_{10}(760p) = 7.614676 - \frac{356.281}{T_{SAT}} \qquad (4)$$

where p is still given in atmospheres. Again, isentropic relations are employed in conjunction with M_∞ to determine the value of $T_{t,SAT}$ that results in free-stream saturation. Next, a total temperature buffer of 2 K is added to this value of T_t.

The third step is to determine if the flow is at a low-power-consumption condition. If it is, then additional free-stream buffering is added. The following guidelines, although somewhat arbitrary, were chosen to provide a margin of safety around the two points with values of $M_{\ell,\max}$ less than 0.70 and with values of $\Delta T(M_\infty)$ equal to -7 K or -8 K. (See previous discussion of fig. 12.) First, this third step is applied only for values of M_∞ less than 0.55. Second, this step is applied only to cases with values of p_t below 4 atm. For values of p_t less than 2 atm, an 8 K buffer is added to the free-stream saturation temperature. For values of p_t between 2 and 4 atm, there is a linear progression from the 8 K buffer at 2 atm to the usual 2 K buffer at 4 atm. (It is suggested that this low power restriction be reexamined in light of the present tunnel capability of selectively closing up to three of the four injectors.)

The fourth, and final, step is to compare the total temperatures calculated during the first three steps and to choose the highest value as the one determining the MOT line.

To see how well the proposed MOT procedure works, the MOT's are compared in figure 24 with data for values of $M_{\ell,\max}$ equal to 0.60, 1.20, 1.30, 1.40, and 1.70. Again, the data shown for comparison are those whose values of $M_{\ell,\max}$ are within ± 0.03 of the stated value of $M_{\ell,\max}$. Since a value of M_∞ had to be specified in order to determine the MOT line, some of the data may have had their specific values of M_∞ above or below the nominal value. However, onset conditions where effects occurred at total temperatures below free-stream saturation are again plotted with flagged symbols. The saturation boundaries for the nominal free stream and local Mach numbers are also shown as dashed-line curves.

Figure 24(a) shows the low Mach number onset points that were involved in the discussion of figure 12. As seen, the third step in the MOT procedure extends the MOT line out and around the points where onset occurred above local saturation temperature. This author is reluctant to reduce this large buffer in the third step because of a lack of data addressing the low-power boundary problem. Figure 24(b) shows the data for $M_{\ell,\max} = 1.20$ and clearly shows a comfortable difference between the MOT and the actual onset data. Figure 24(c) shows the data for $M_{\ell,\max} = 1.30$ and shows that some of the data did come within 1 K or 2 K of the MOT. Figure 24(d) displays the data for $M_{\ell,\max} = 1.40$ and again shows the MOT at temperatures higher than those of the data. Finally, figure 24(e) displays the data for $M_{\ell,\max} = 1.70$ and shows satisfactory MOT performance.

Impact of MOT On Maximum Reynolds Number Capability

After determining a procedure to establish the MOT, it is now possible to assess the quantitative

influence that the MOT will have on maximum Reynolds number capability of the tunnel. For a first approximation, flow equations assuming an ideal diatomic gas combined with Sutherland's formula for viscosity (in SI units)

$$\mu = (1.378 \times 10^{-6}) \frac{\sqrt{T}}{1 + (103/T)} \qquad (5)$$

are used to calculate two free-stream Reynolds numbers based on M_∞, p_t, and either the total temperature as predicted by the MOT procedure (denoted by MOT T_t) or the $T_{t,\mathrm{SAT}}$ corresponding to saturation at the maximum local Mach number. A percentage increase in Reynolds number capability by operating at the MOT T_t is determined by subtracting the $T_{t,\mathrm{SAT}}$ value from the MOT T_t value and dividing by the value calculated at $T_{t,\mathrm{SAT}}$. The results are shown in figure 25(a) for the same free-stream and local Mach number combinations displayed in figure 24. For a more precise approximation, a second calculation was done using a computer program written with a Beattie-Bridgeman equation-of-state description of nitrogen gas, as reported in reference 9. The results of this second calculation are shown in figure 25(b) and are very similar to the ideal calculation, which suggests that assuming that nitrogen is an ideal diatomic gas is sufficiently accurate for these calculations.

The first thing to observe in figure 25 is that one must operate above $M_{\ell,\max}$ saturation for the case of $M_\infty = 0.45$. The unusual shape of curve (a) is due to different buffer magnitudes as a function of p_t. The nearly straight behavior of curve (b) is the result of the MOT being determined by the free-stream saturation boundary exclusively. The change in slope of curve (c) near p_t equal to 1 atm is due to a change from the MOT being determined by the curve fit to Sivier's analysis with a buffer for p_t above about 1.4 atm to the MOT being determined by the free-stream saturation curve with a buffer below that value of p_t. In general, the higher the total pressure at which the tunnel is operated, the less gain is possible before condensation occurs. To summarize, for the conditions analyzed with M_∞ greater than 0.55, predicted increases in Reynolds number vary from 7 to 22 percent above those associated with operating at local saturation temperatures, depending on p_t, M_∞, and $M_{\ell,\max}$.

Impact of MOT on Liquid Nitrogen Consumption

In addition to increasing maximum Reynolds number capability, MOT's below local saturation can be important when determining the most cost-effective means of running the tunnel for a value of Reynolds number that is within a tunnel operating envelope. Since cryogenic tunnels use both increasing tunnel pressure and decreasing tunnel temperature to increase unit Reynolds number capability, a lower tunnel temperature means less pressure is needed to achieve a particular value of Reynolds number. Since operating costs are primarily linked to tunnel pressure, direct on-point operating expenses can, therefore, be minimized by operating at the MOT in order to maximize the benefits of low temperatures while reducing required operating pressures.

As was done in determining increases in percent of Reynolds number capability, both an ideal-gas analysis or a real-gas analysis can be used to establish the rate of liquid nitrogen consumption. Adcock and Ogburn in reference 25 present calculations for power use that assume an ideal diatomic gas, a fully real-gas description of nitrogen, or a hybrid analysis involving use of the compressibility of nitrogen gas. It is reported in the reference that the hybrid analysis is accurate to within ± 0.5 percent of the fully real-gas calculation. For the present study, both the ideal and hybrid sets of equations given in reference 25 are used in conjunction with a description of the cooling capacity of liquid nitrogen (see ref. 26) to evaluate the potential savings in LN_2 required when operating at the MOT temperature in contrast to operating at the same Reynolds number but at the local saturation temperature. The results are presented in figure 26. As before, there is no significant difference between the fully ideal calculation and the more exact analysis. The main features of either plot are, first, their general similarity to figure 25. Second, it appears that for the flows with M_∞ greater than 0.55, savings in on-point operating costs can vary from 8 to 22 percent, depending on p_t, M_∞, and $M_{\ell,\max}$.

Establishing MOT For Different Tunnels

The next challenge is to determine if the above MOT procedure, as determined for the 0.3-m TCT, is also appropriate for other transonic cryogenic tunnels, such as the National Transonic Facility (NTF) at the Langley Research Center. Although experiments in the NTF are planned to examine the onset of condensation over a wide range of tunnel conditions, a few general comments can be made about tunnel-to-tunnel comparisons. The most important factor is background seed-particle distribution, which can result from oil leaks, impurities in the injected liquid, dirt, etc. If a second tunnel has seed particles of a higher number density than that of the 0.3-m TCT, then growth on those seed particles could dominate the condensation processes not only below

free-stream saturation but also locally over the model even before the free stream becomes saturated. If this occurs, the curve fit to Sivier's analysis, which is based on homogeneous nucleation, no longer applies nor do the comments concerning negligible length effects. (See ref. 3 for more details.) On the other hand, if seed-particle-number density is less than that of the 0.3-m TCT, the above MOT lines should be reasonable boundaries for the second tunnel as well. The second most important factor is the efficiency of the liquid nitrogen atomization. Just as low power consumption was determined to cause condensation onset at relatively higher temperatures in the 0.3-m TCT because of inefficient atomization, the same could be expected if another tunnel has the same difficulty.

Summary of Results

The results of the airfoil condensation studies in the Langley 0.3-Meter Transonic Cryogenic Tunnel (0.3-m TCT) utilizing the NACA 0012-64, NPL 9510, NACA 0012, NASA SC(3)-0712(B), and the smaller- and larger-chord versions of the CAST 10-2/DOA 2 airfoil can be summarized as follows:

1. The most important parameter to describe and correlate the data is the value of maximum local Mach number $M_{\ell,\max}$. This parameter was also found to be most helpful in determining and understanding when to expect condensation onset to result from growth of condensate on preexisting seed particles in the free stream upstream of the model or from homogeneous nucleation occurring over the airfoils themselves.

2. In general, effects stemming from condensation growth in the free stream were important only when $M_{\ell,\max}$ was equal to or less than 1.20. For values of $M_{\ell,\max}$ greater than 1.20, homogeneous nucleation was dominant.

3. A simple curve fit to the results of a computer study by Sivier seems to give a good prediction of condensation effects due to homogeneous nucleation for the six airfoils used in this study.

4. A simple procedure is presented to predict minimum operating temperatures (MOT's) in the 0.3-m TCT, and comments are addressed to the operation in other transonic cryogenic tunnels, such as the National Transonic Facility (NTF) at the Langley Research Center.

5. At values of free-stream Mach number M_∞ less than 0.55, the MOT boundaries can occur above local saturation temperatures because of the potentially poor atomization of the injected liquid nitrogen at low tunnel operating power. (This poor atomization can result in unevaporated liquid nitrogen droplets reaching the test section and causing effects through either their own continued evaporation or through their wetting of surfaces.)

6. Reynolds number capability increases from 7 to 22 percent are predicted by the MOT's for various flow conditions with M_∞ greater than 0.55 because of the ability to test below local saturation temperature before the onset of condensation effects.

7. Decreases in on-point liquid nitrogen consumption between 8 and 22 percent are predicted by the MOT's for values of M_∞ greater than 0.55.

8. Contrary to a calculation by Wagner, drag measurements do not appear to be a sensitive indicator of condensation effects.

NASA Langley Research Center
Hampton, VA 23665-5225
October 30, 1985

References

1. Hall, Robert M.; and Kramer, Susan A.: *A Review of "At Rest" Droplet Growth Equations for Condensing Nitrogen in Transonic Cryogenic Wind Tunnels.* NASA TM-78821, 1979.
2. Hall, Robert M.: *Onset of Condensation Effects With an NACA 0012-64 Airfoil Tested in the Langley 0.3-Meter Transonic Cryogenic Tunnel.* NASA TP-1385, 1979.
3. Hall, Robert M.: Real Gas Effects II—Influence of Condensation on Minimum Operating Temperatures of Cryogenic Wind Tunnels. *Cryogenic Wind Tunnels*, AGARD-LS-111, May 1980, pp. 7–1—7–21.
4. Hall, Robert M.: Onset of Condensation Effects in Cryogenic Wind Tunnels. *High Reynolds Number Research—1980*, L. Wayne McKinney and Donald D. Baals, eds., NASA CP-2183, 1981, pp. 93–104.
5. Hall, Robert M.: Pre-Existing Seed Particles and the Onset of Condensation in Cryogenic Wind Tunnels. AIAA-84-0244, Jan. 1984.
6. Jenkins, Renaldo V.: *Reynolds Number Tests of an NPL 9510 Airfoil in the Langley 0.3-Meter Transonic Cryogenic Tunnel.* NASA TM-85663, 1983.
7. Adcock, Jerry B.: *Real-Gas Effects Associated With One-Dimensional Transonic Flow of Cryogenic Nitrogen.* NASA TN D-8274, 1976.
8. Hall, Robert M.: Real Gas Effects I—Simulation of Ideal Gas Flow by Cryogenic Nitrogen and Other Selected Gases. *Cryogenic Wind Tunnels*, AGARD-LS-111, May 1980, pp. 5–1—5–16.
9. Hall, Robert M.; and Adcock, Jerry B.: *Simulation of Ideal-Gas Flow by Nitrogen and Other Selected Gases at Cryogenic Temperatures.* NASA TP-1901, 1981.
10. Wagner, Bernhard.: *Estimation of Simulation Errors and Investigations of Operating Range Extensions for the European Transonic Windtunnel ETW.* BMFT-FB-W 82-003, Bundesministerium für Forschung und Technologie (Postfach, Bonn (Germany)), July 1982.

11. Hall, Robert M.: Studies of Condensation Effects on Airfoil Testing in a Transonic Cryogenic Tunnel. AIAA-85-0229, Jan. 1985.
12. Ray, Edward J.; Ladson, Charles L.; Adcock, Jerry B.; Lawing, Pierce L.; and Hall, Robert M.: *Review of Design and Operational Characteristics of the 0.3-Meter Transonic Cryogenic Tunnel.* NASA TM-80123, 1979.
13. Ladson, Charles L.; and Kilgore, Robert A.: *Instrumentation for Calibration and Control of a Continuous-Flow Cryogenic Tunnel.* NASA TM-81825, 1980.
14. Ladson, Charles L.; and Brooks, Cuyler W., Jr.: *Development of a Computer Program To Obtain Ordinates for NACA 4-Digit, 4-Digit Modified, 5-Digit, and 16-Series Airfoils.* NASA TM X-3284, 1975.
15. Johnson, William G., Jr.; Hill, Acquilla S.; and Eichmann, Otto: *Pressure Distributions From High Reynolds Number Tests of a NASA SC(3)-0712(B) Airfoil in the Langley 0.3-Meter Transonic Cryogenic Tunnel.* NASA TM-86370, 1985.
16. Dress, David A.; Johnson, Charles B.; McGuire, Peggy D.; Stanewsky, Egon; and Ray, Edward J.: *High Reynolds Number Tests of the CAST 10-2/DOA 2 Airfoil in the Langley 0.3-Meter Transonic Cryogenic Tunnel—Phase I.* NASA TM-84620, 1983.
17. Dress, David A.; Stanewsky, Egon; McGuire, Peggy D.; and Ray, Edward J.: *High Reynolds Number Tests of the CAST 10-2/DOA 2 Airfoil in the Langley 0.3-Meter Transonic Cryogenic Tunnel—Phase II.* NASA TM-86273, 1984.
18. Wegener, P. P.; and Mack, L. M.: Condensation in Supersonic and Hypersonic Wind Tunnels. *Advances in Applied Mechanics*, Volume V, H. L. Dryden and Th. von Kármán, eds., Academic Press, Inc., 1958, pp. 307–447.
19. Gyarmathy, G.: Condensation in Flowing Steam. *Two-Phase Steam Flow in Turbines and Separators*, M. J. Moore and C. H. Sieverding, eds., Hemisphere Pub. Corp., c.1976, pp. 127–189.
20. Sivier, Kenneth R.: *Digital Computer Studies of Condensation in Expanding One-Component Flows.* ARL 65-234, U.S. Air Force, Nov. 1965. (Available from DTIC as AD 628 543.)
21. Dotson, Edward H.: *Homogeneous Nucleation and Droplet Growth in Nitrogen.* NASA CR-172206, 1983.
22. Arthur, P. D.; and Nagamatsu, H. T.: *Effects of Impurities on the Supersaturation of Nitrogen in a Hypersonic Nozzle.* Memo. No. 7 (Contract No. DA-04-495-Ord-19), GALCIT, Mar. 1, 1952.
23. Dodge, Barnett F.; and Davis, Harvey N.: Vapor Pressure of Liquid Oxygen and Nitrogen. *J. American Chem. Soc.*, vol. 49, Mar. 1927, pp. 610–620.
24. Frels, W.; Smith, D. R.; and Ashworth, T.: Vapour Pressure of Nitrogen Below the Triple Point. *Cryogenics*, vol. 14, no. 1, Jan. 1974, pp. 3–7.
25. Adcock, Jerry B.; and Ogburn, Marilyn E.: *Power Calculations for Isentropic Compressions of Cryogenic Nitrogen.* NASA TN D-8389, 1977.
26. Kilgore, Robert A.; and Adcock, Jerry B.: *Specific Cooling Capacity of Liquid Nitrogen.* NASA TM X-74015, 1977.

TABLE I. AIRFOILS TESTED

Airfoil[a]	Class	Chord, m
NACA 0012-64	Conventional	0.137
NPL 9510	"Peaky"[b]	.152
NACA 0012	Conventional	.152
NASA SC(3)-0712(B)	Supercritical	.152
CAST 10-2/DOA 2	Supercritical	.152
CAST 10-2/DOA 2	Supercritical	.076

[a]The 10-2 airfoil has both $c = 0.152$ m and $c = 0.076$ m.
[b]Airfoil designed with a peak in the upper-surface pressure distribution.

TABLE II. AIRFOIL ABBREVIATIONS USED IN FIGURES

Complete airfoil designation[a]	Abbreviation in figures
NACA 0012-64	0012-64
NPL 9510	9510
NACA 0012	0012
NASA SC(3)-0712(B)	0712(3)
CAST 10-2/DOA 2	0.152 10-2
CAST 10-2/DOA 2	0.076 10-2

[a]The 10-2 airfoil has both $c = 0.152$ m and $c = 0.076$ m.

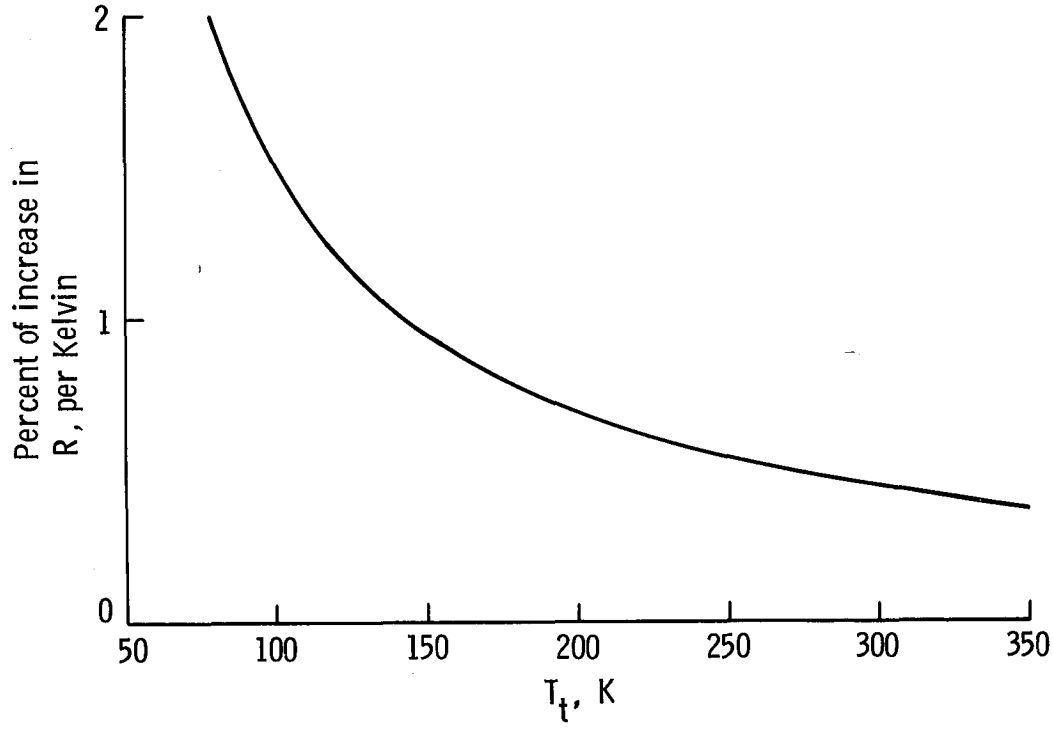

Figure 1. Percent of increase in unit Reynolds number for each Kelvin drop in total temperature. $M_\infty = 1.00$; $p_t = 1.0$ atm.

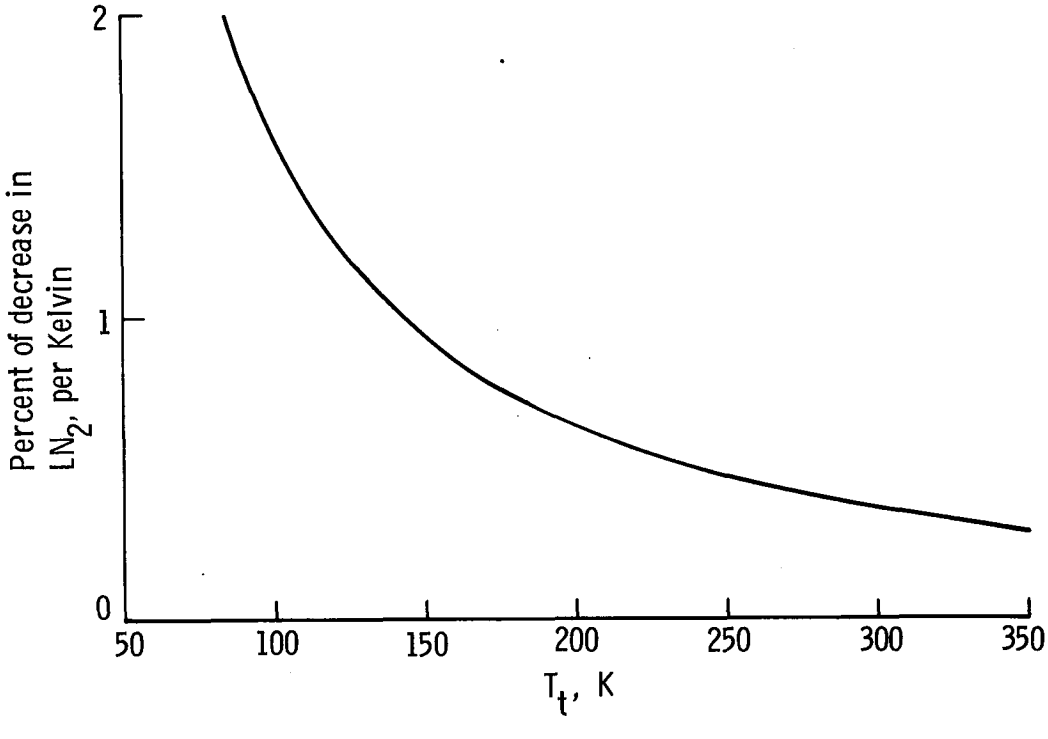

Figure 2. Percent of decrease in liquid nitrogen consumption for each Kelvin drop in total temperature. $M_\infty = 1.00$; $R = 120 \times 10^6$ per meter.

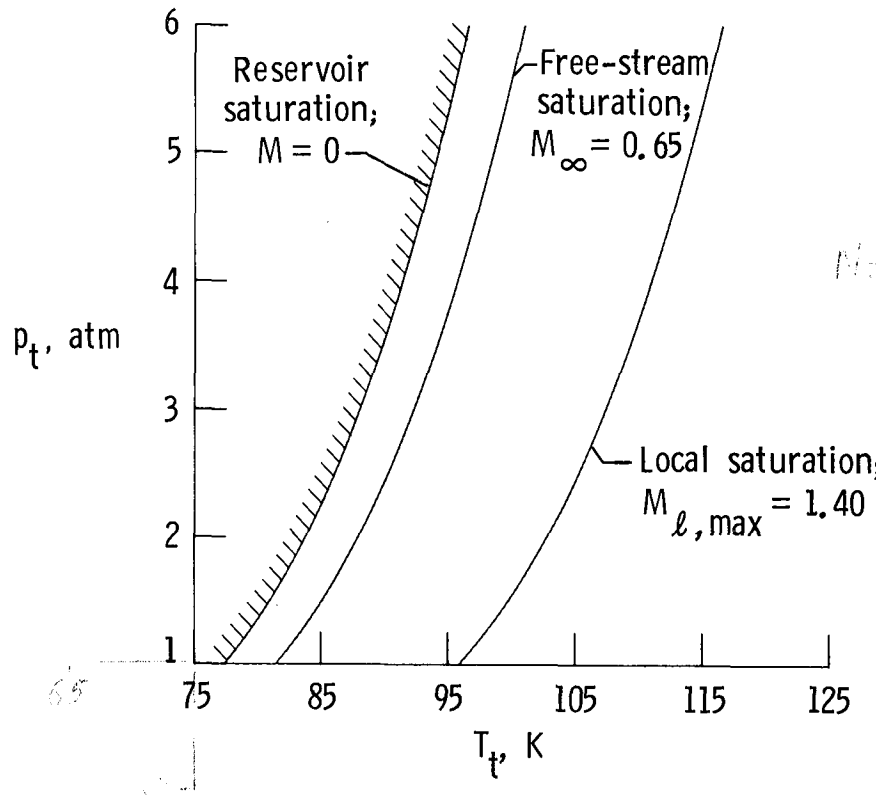

Figure 3. Saturation temperature boundaries for stated values of local, free-stream, and reservoir Mach numbers.

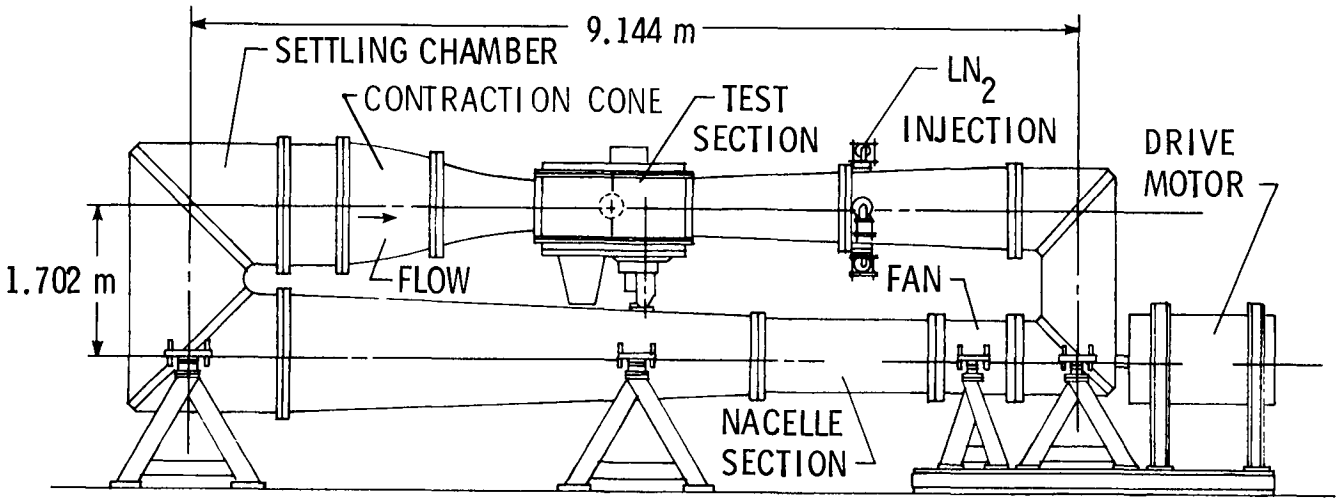

Figure 4. Schematic diagram of Langley 0.3-Meter Transonic Cryogenic Tunnel.

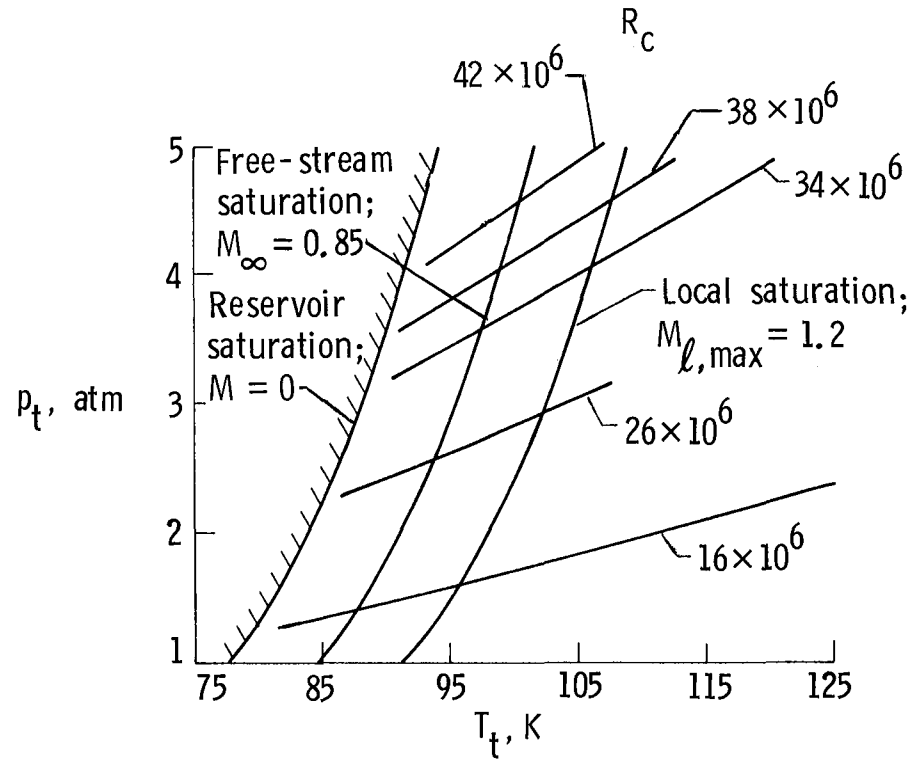

Figure 5. Paths of constant R_c for NACA 0012-64 airfoil. $M_\infty = 0.85$; $M_{\ell,\max} = 1.20$; $\alpha = 0°$.

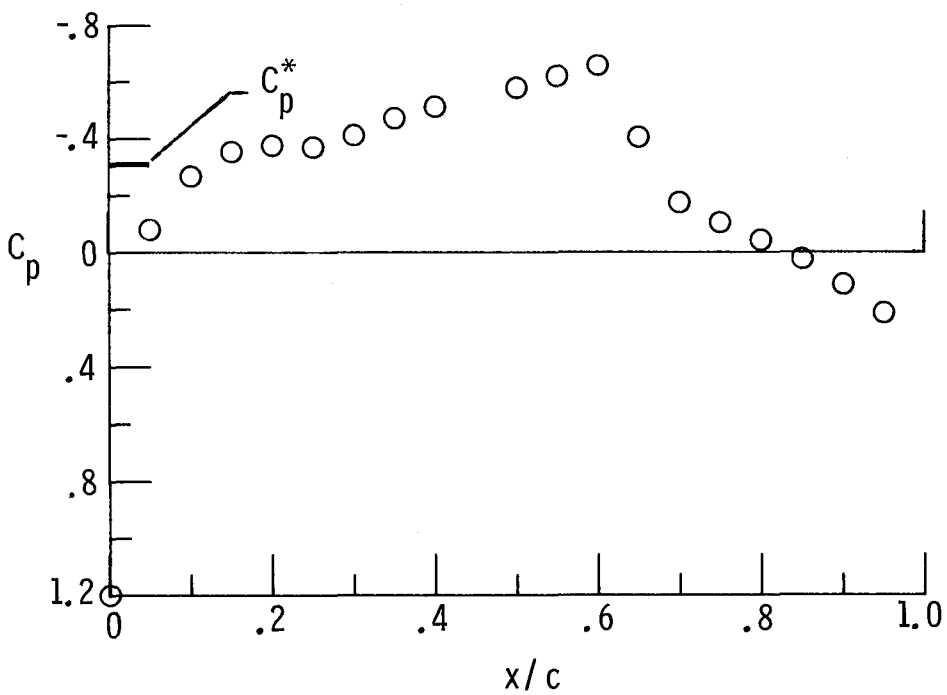

Figure 6. Pressure distribution before onset of condensation effects for NACA 0012-64 airfoil. $M_\infty = 0.85$; $M_{\ell,\max} = 1.20$; $\alpha = 0°$; $R_c = 16 \times 10^6$.

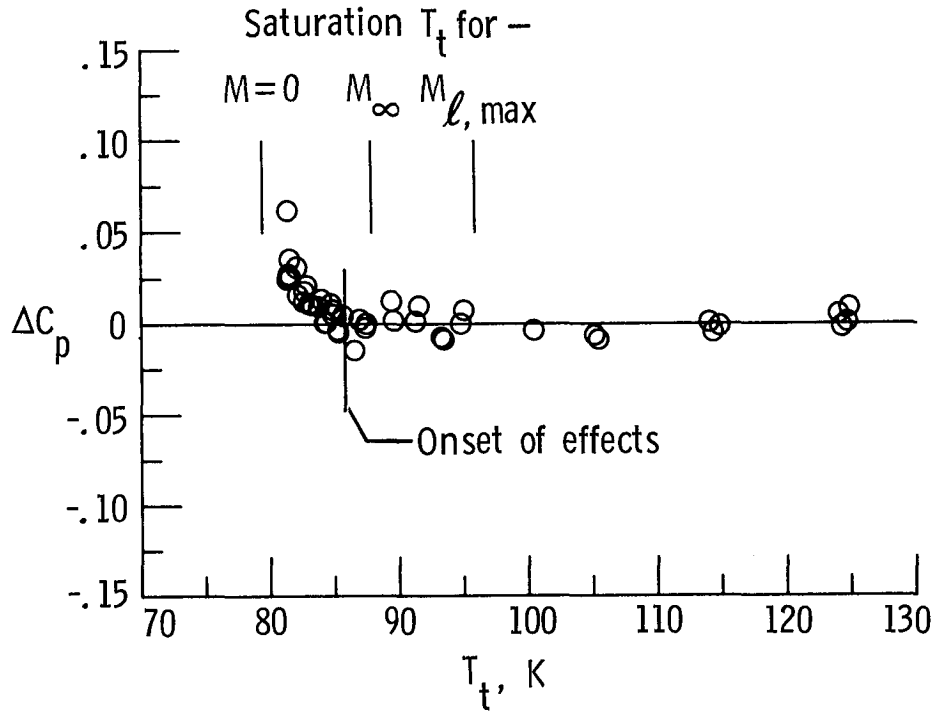

Figure 7. Sample plot of ΔC_p for orifice at which $M_{\ell,\max}$ occurs. NACA 0012-64 airfoil; $M_\infty = 0.85$; $M_{\ell,\max} = 1.20$; $\alpha = 0°$; $R_c = 16 \times 10^6$; $x/c = 0.60$.

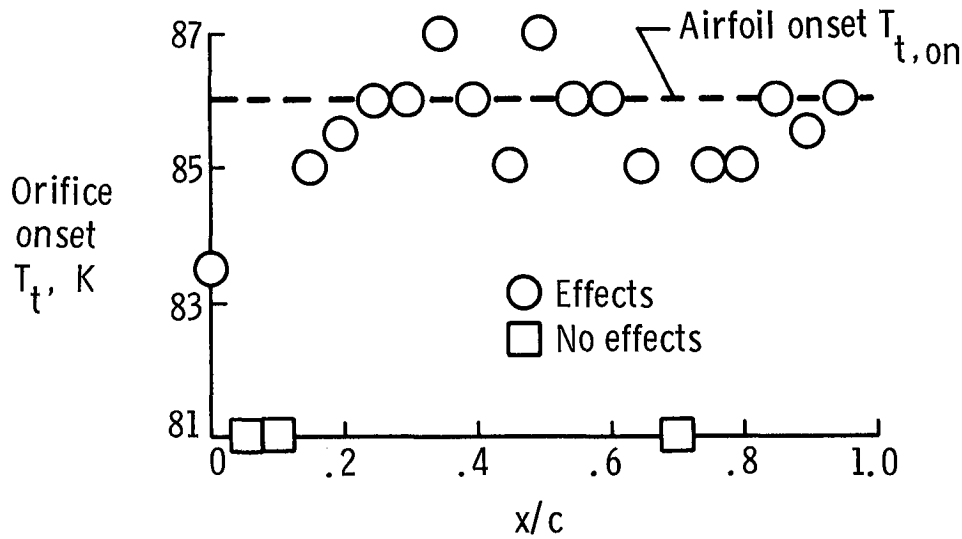

Figure 8. Orifice onset T_t and resulting airfoil onset $T_{t,\text{on}}$ for path with $R_c = 16 \times 10^6$. Square symbols signify orifices where value of pressure did not change because of condensation onset.

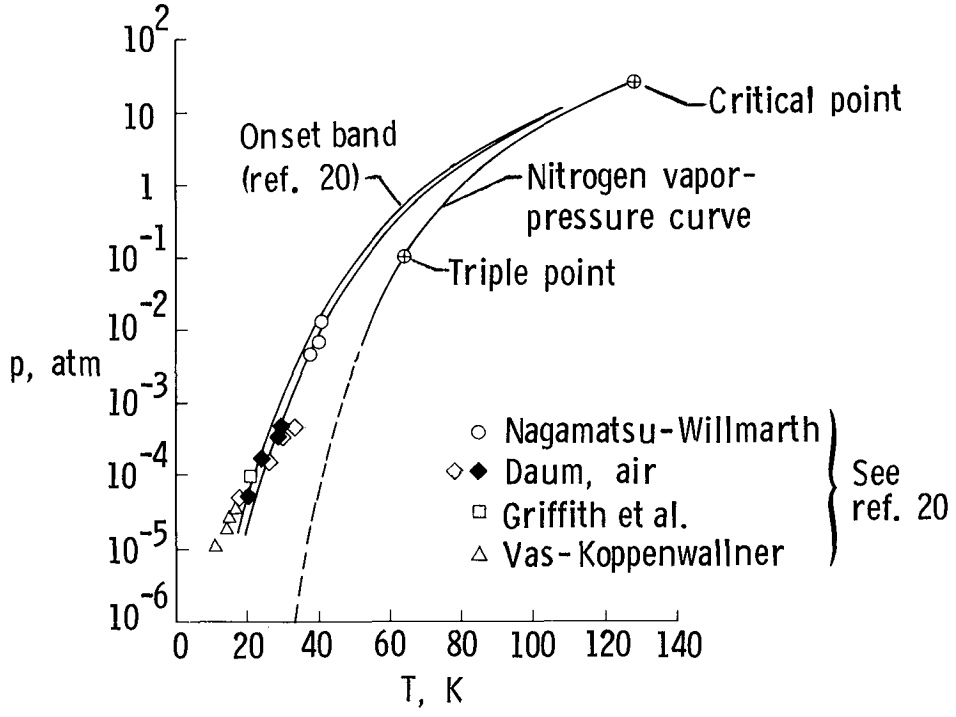

Figure 9. Onset band predicted by Sivier for homogeneous nucleation with nitrogen (from ref. 20). Daum's original data are represented by ◇; data corrected by Sivier in reference 20 are represented by ◆.

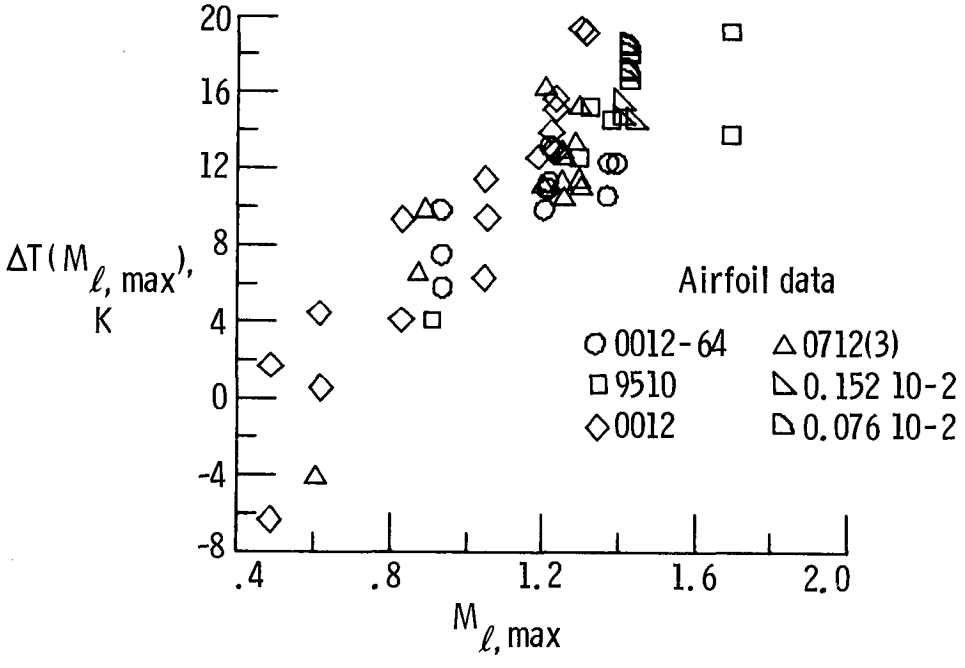

Figure 10. Supercooling based on maximum local Mach number plotted against maximum local Mach number. Data included for all airfoils. See table II for airfoil clarification.

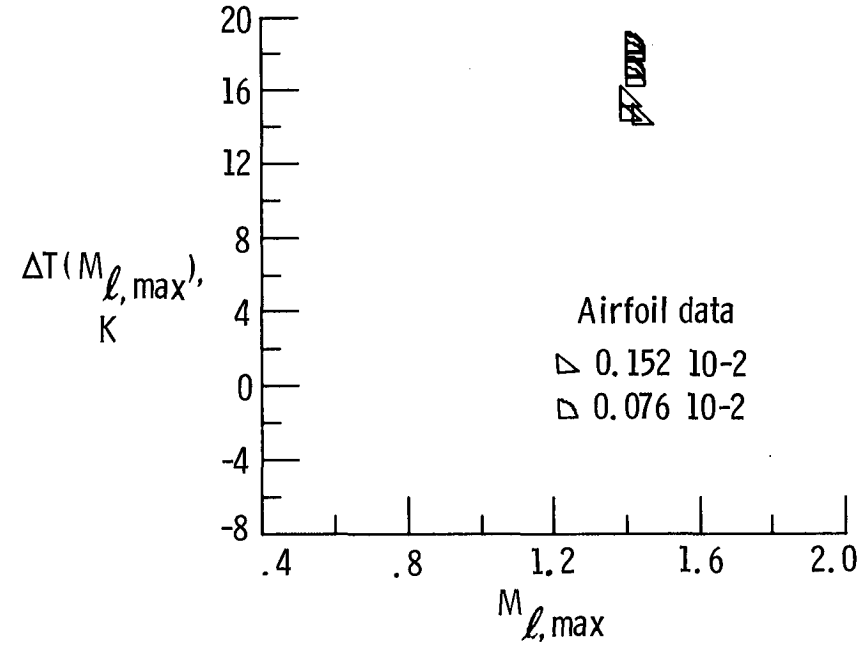

Figure 11. Differences in supercooling for two tests with different chords. CAST 10-2/DOA 2 airfoil; $M_\infty = 0.65$; $M_{\ell,\max} = 1.40$; $\alpha = 6°$. See table II for airfoil clarification.

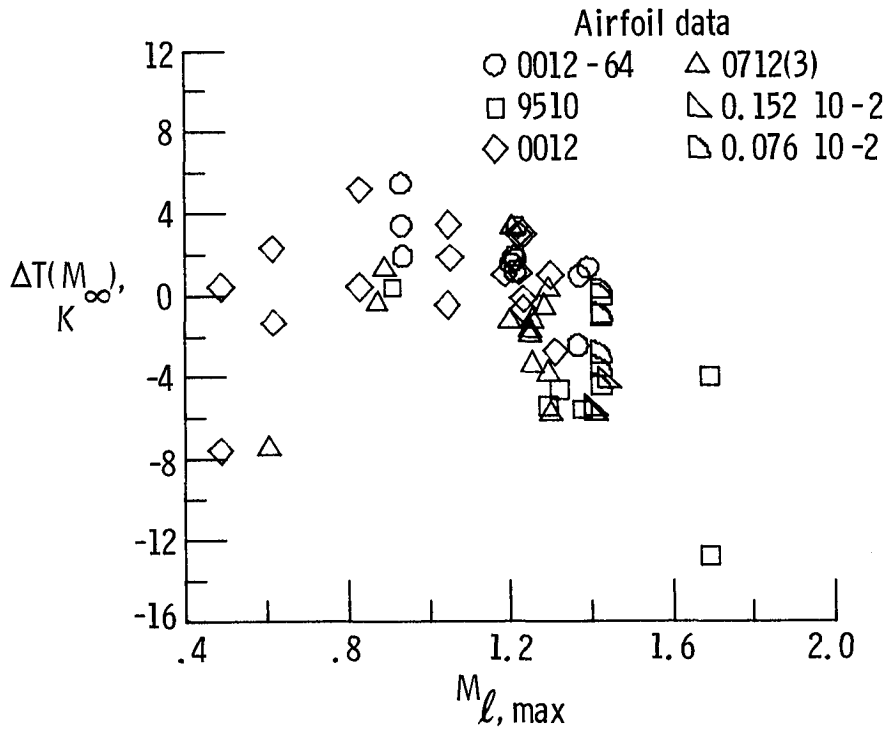

Figure 12. Supercooling based on M_∞ as a function of maximum local Mach number. See table II for airfoil clarification.

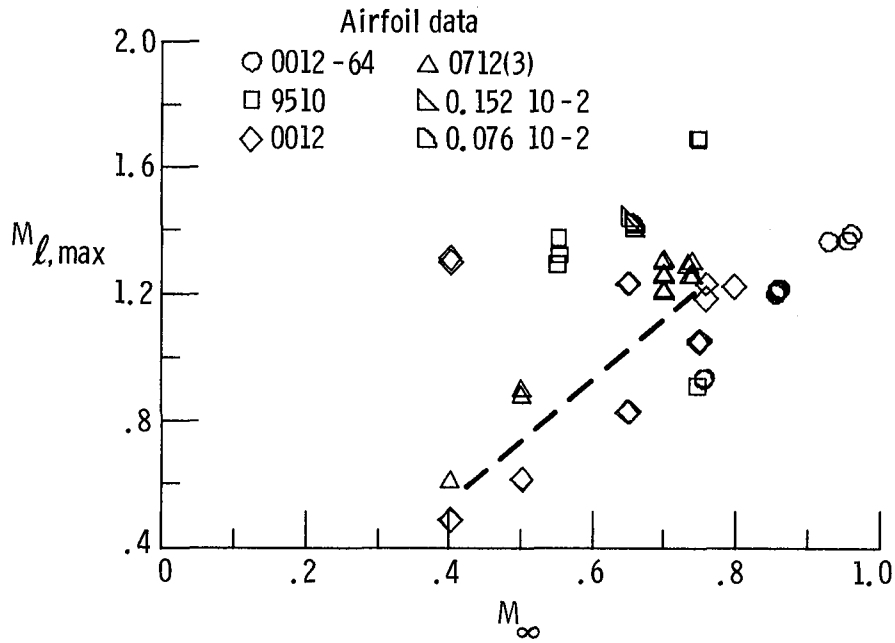

Figure 13. Relationship between $M_{\ell,\max}$ and M_∞. Dashed line represents nearly linear relationship between test values of maximum local and free-stream Mach numbers for values of maximum local Mach number less than 1.2. See table II for airfoil clarification.

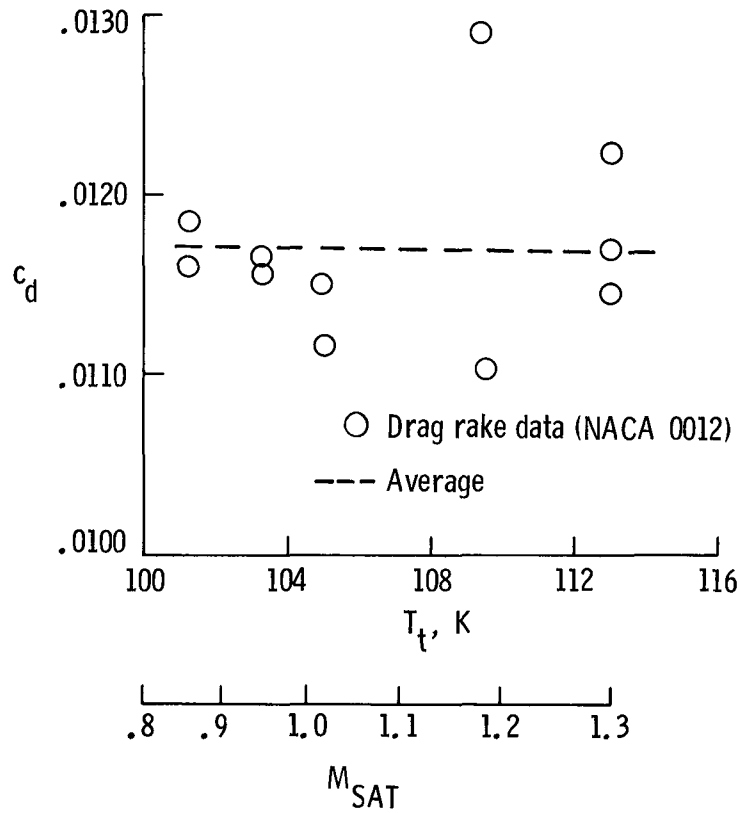

Figure 14. c_d as a function of either T_t or M_{SAT} at $R_c = 45.3 \times 10^6$. $M_\infty = 0.76$; $M_{\ell,\max} = 1.28$; $\alpha = 2.0°$.

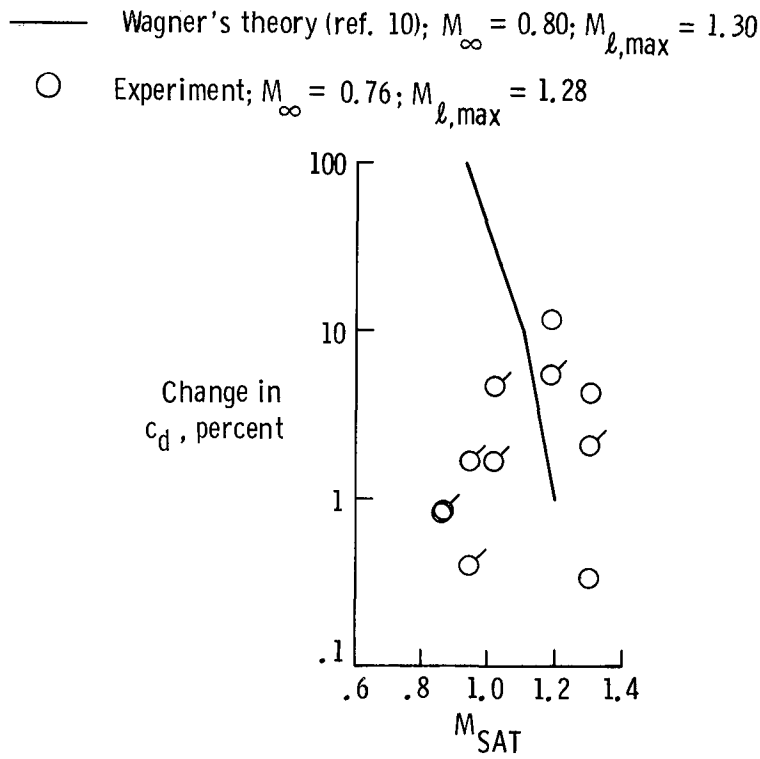

Figure 15. Comparison of experimental and theoretical changes in section drag coefficient for NACA 0012 airfoil. Flagged symbols represent decreases in measured drag.

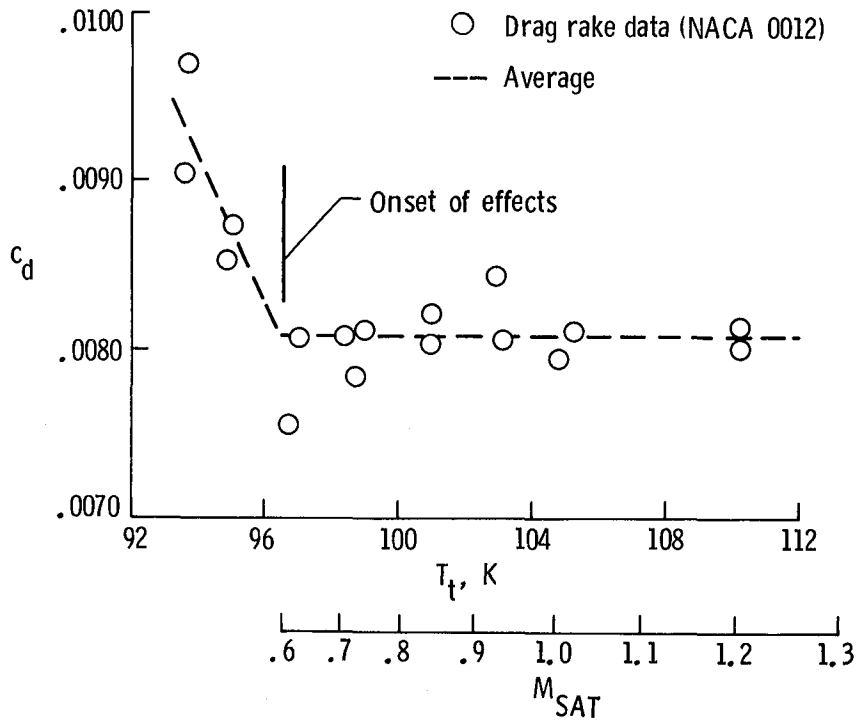

Figure 16. c_d as a function of either T_t or M_{SAT} at $R_c = 41.1 \times 10^6$. $M_\infty = 0.65$; $M_{\ell,max} = 1.23$; $\alpha = 4.5°$.

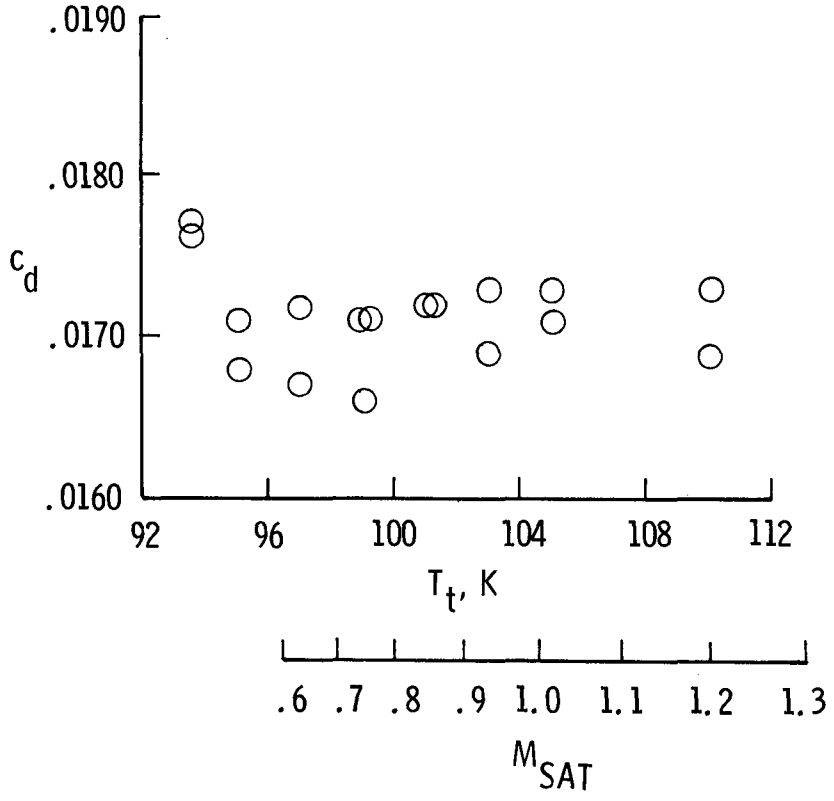

Figure 17. Integrated surface pressure drag for NACA 0012 airfoil. $M_\infty = 0.65$; $M_{\ell,\max} = 1.23$; $\alpha = 4.5°$; $R_c = 41.1 \times 10^6$.

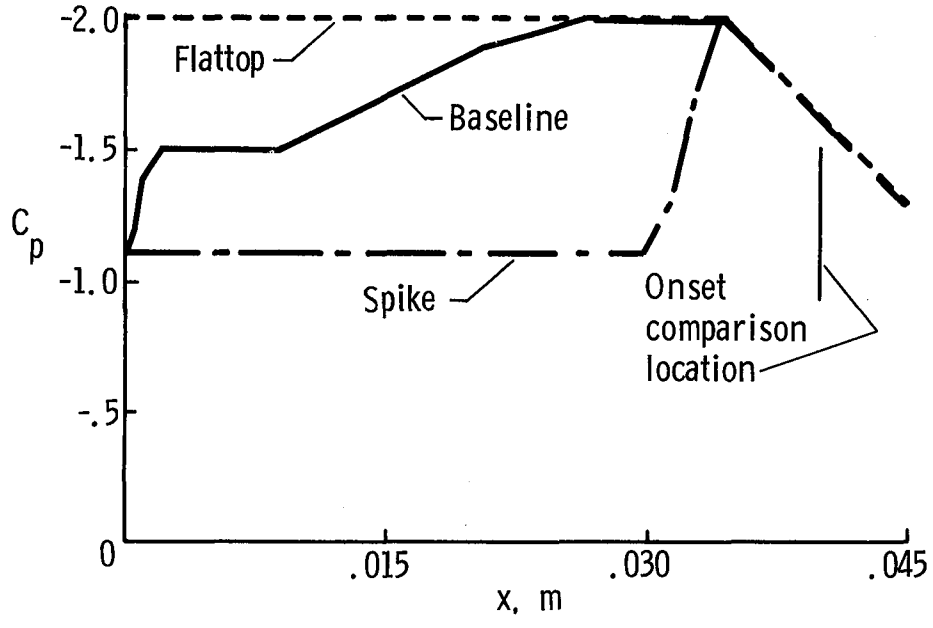

Figure 18. Three hypothetical pressure distributions used for sensitivity analysis.

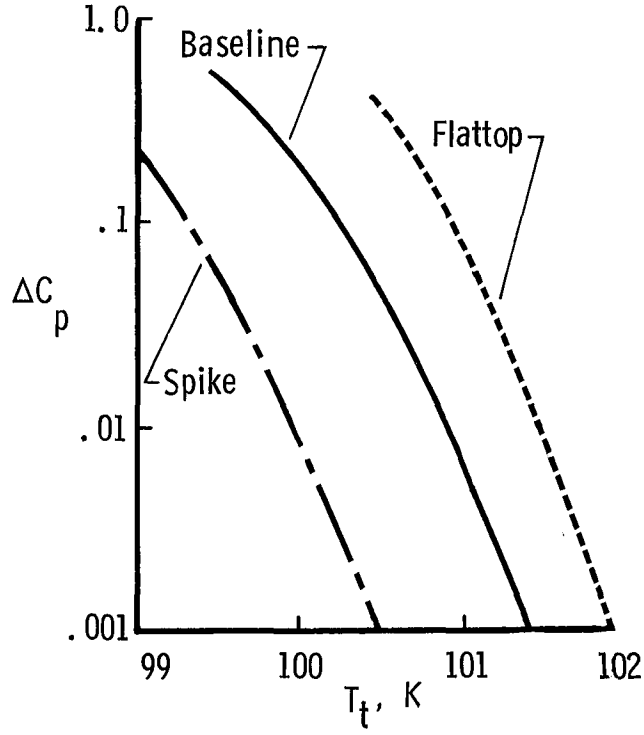

Figure 19. Predicted magnitude of differences in C_p due to condensation as a function of T_t for different pressure distributions. $p_t = 5.0$ atm.

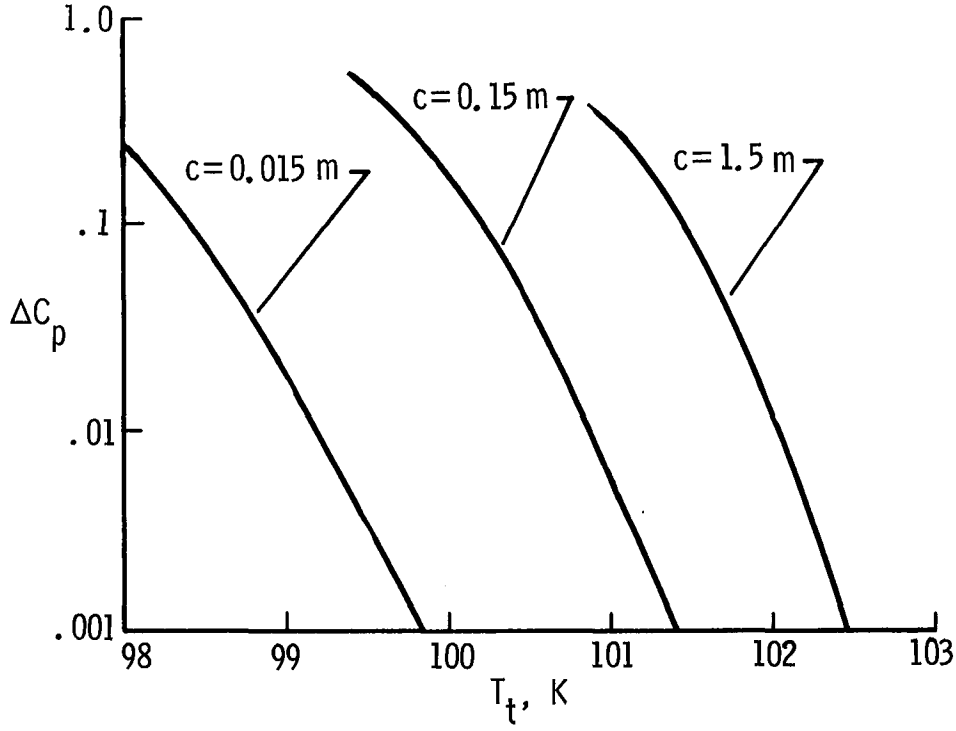

Figure 20. Predicted magnitude of differences in C_p due to condensation as a function of T_t for different airfoil chords. $p_t = 5.0$ atm.

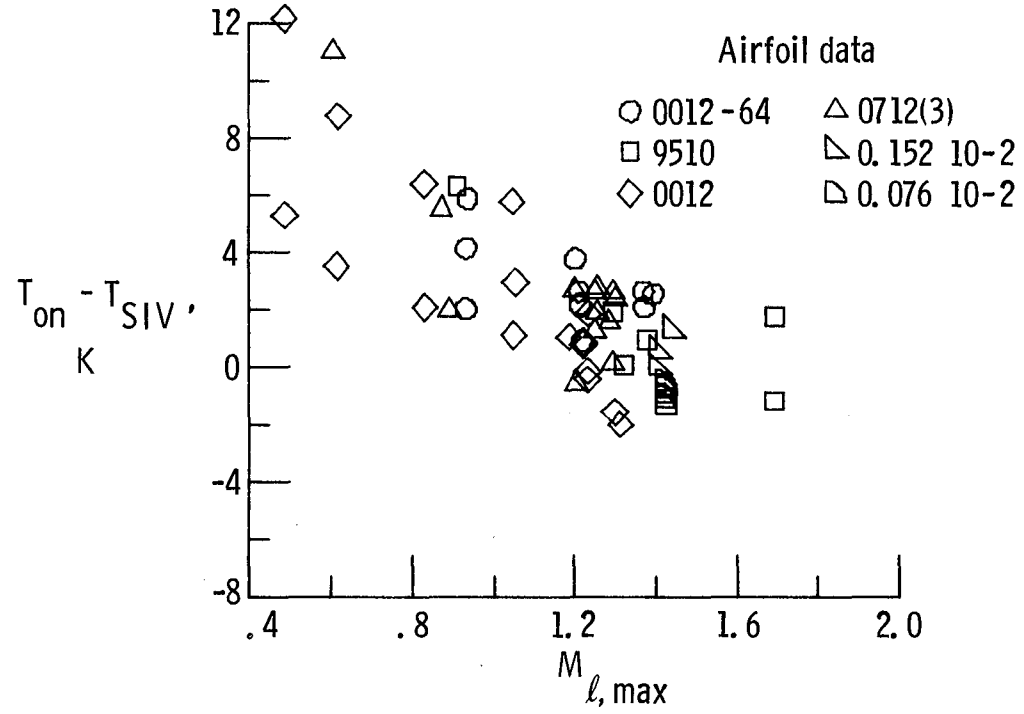

Figure 21. Differences in static temperature at onset between experiment and curve fit to Sivier's analysis as a function of $M_{\ell,\max}$. See table II for airfoil clarification.

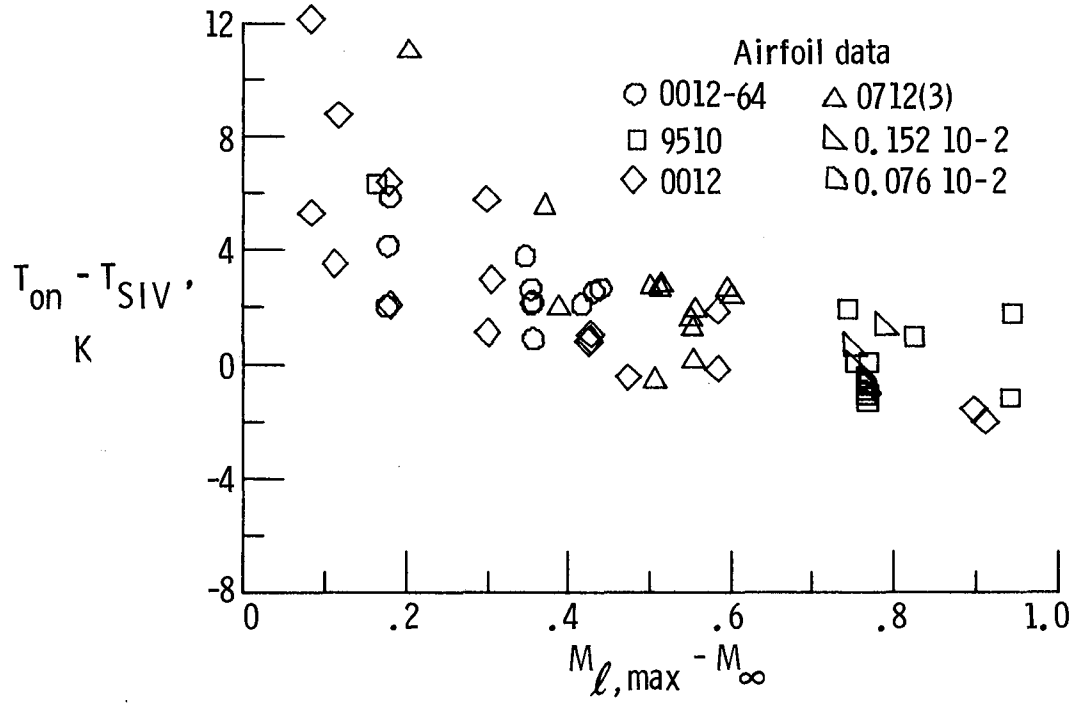

Figure 22. Differences in static temperature at onset between experiment and curve fit to Sivier's analysis as a function of $M_{\ell,\max} - M_{\infty}$. See table II for airfoil clarification.

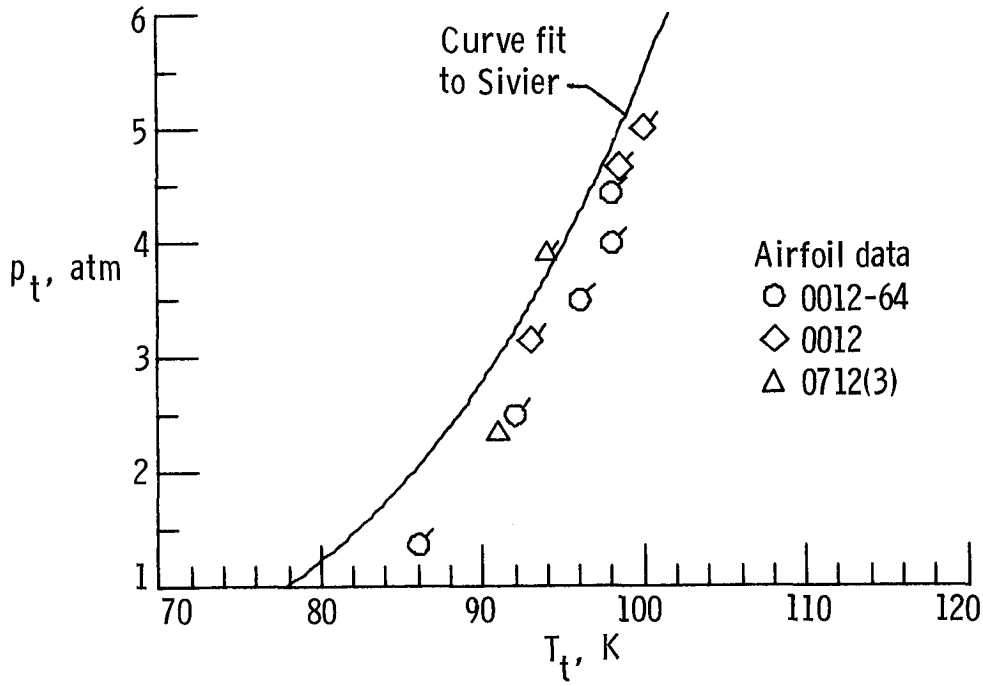

(a) $M_{\ell,\max} = 1.20$.

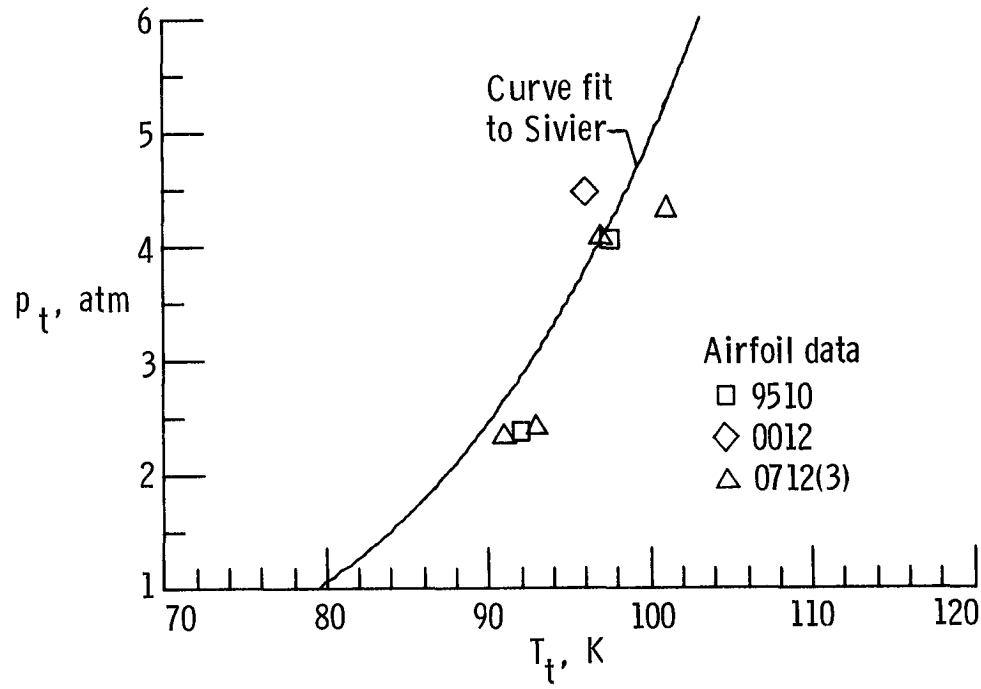

(b) $M_{\ell,\max} = 1.30$.

Figure 23. Comparison of curve fit to Sivier's analysis with experimental data. Experimental values of $M_{\ell,\max}$ are within ±0.03 of stated value. Flagged symbols identify conditions where onset has occurred below free-stream saturation. See table II for airfoil clarification.

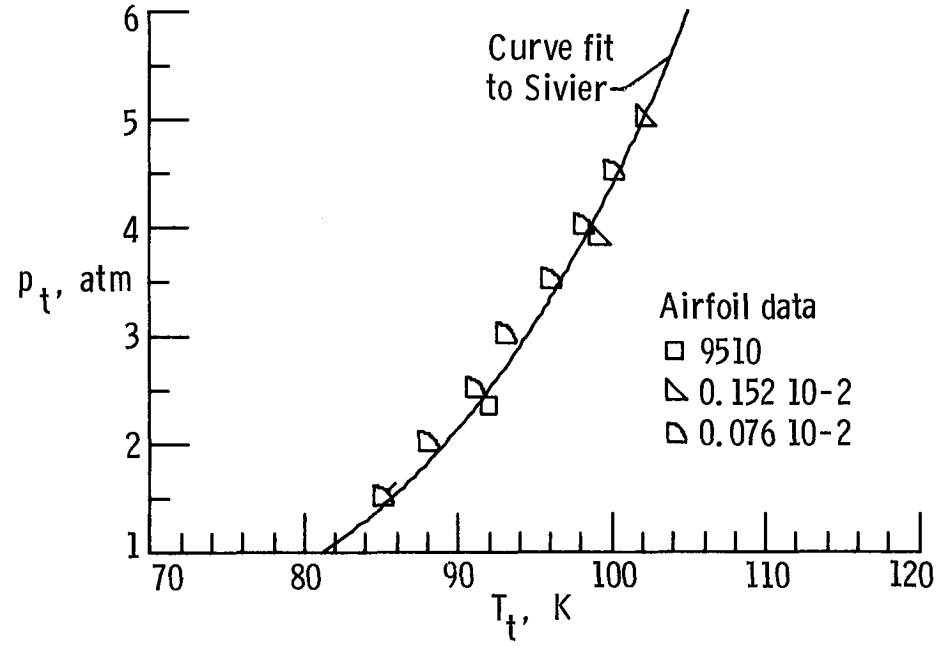

(c) $M_{\ell,\max} = 1.40$.

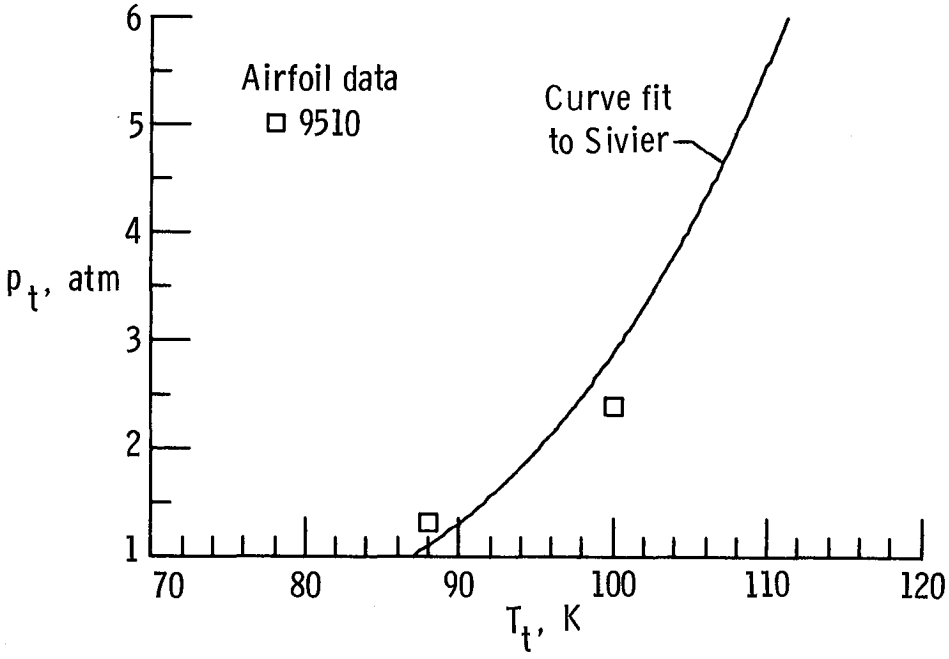

(d) $M_{\ell,\max} = 1.70$.

Figure 23. Concluded.

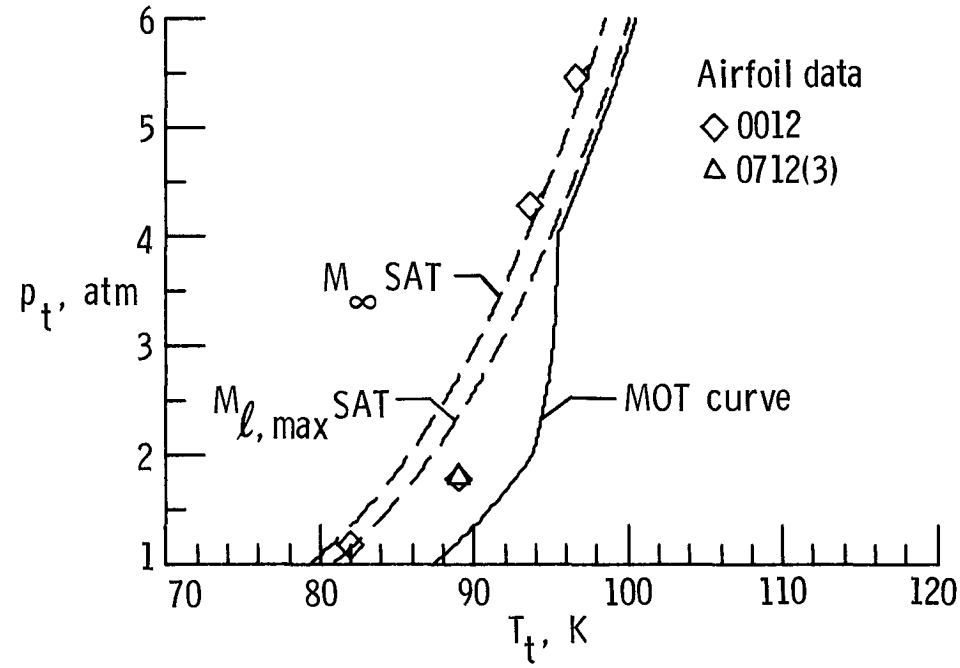

(a) $M_\infty = 0.45$; $M_{\ell,\max} = 0.60$.

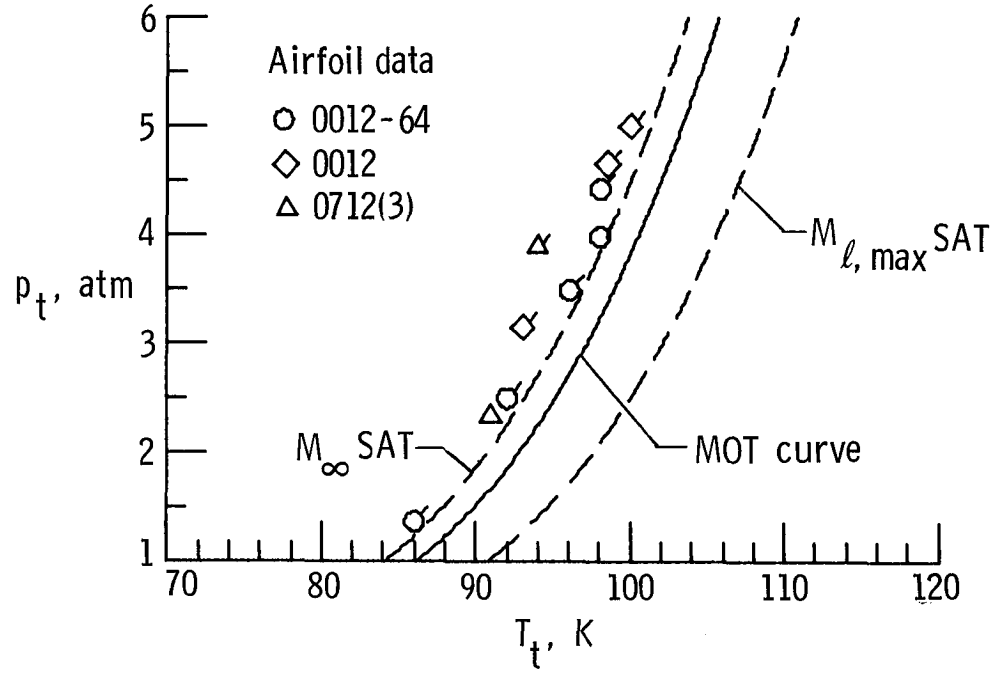

(b) $M_\infty = 0.85$; $M_{\ell,\max} = 1.20$.

Figure 24. Comparison of predicted minimum operating temperatures (MOT's) to airfoil onset data with values of $M_{\ell,\max}$ within ± 0.03 of stated value. Dashed-line curves represent respective saturation curves; flagged symbols identify conditions where onset has occurred at total temperatures below free-stream saturation. See table II for airfoil clarification.

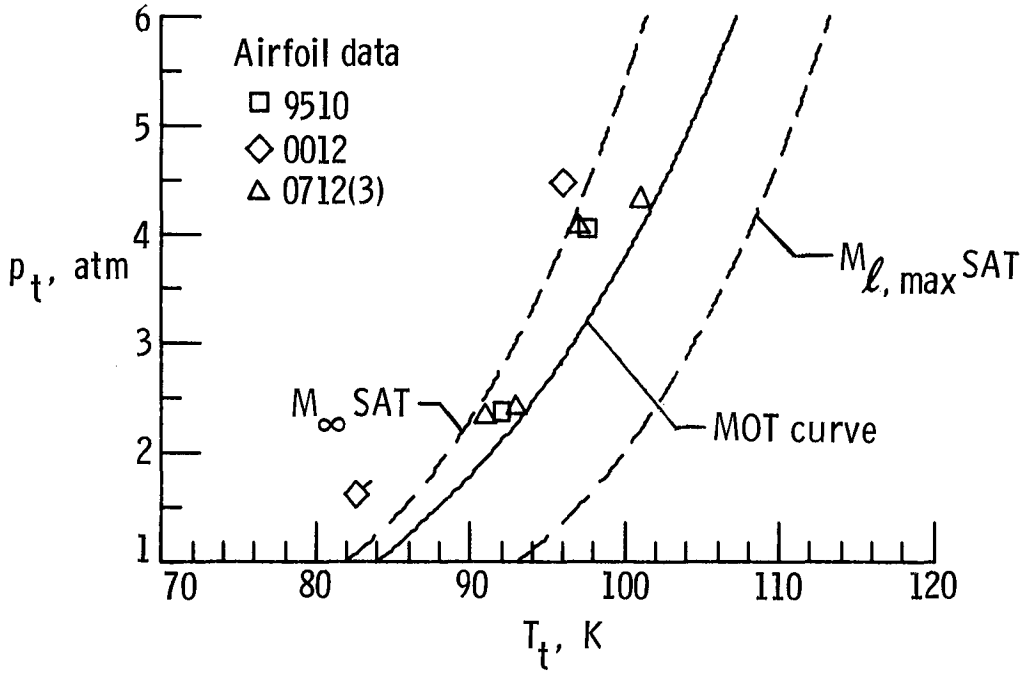

(c) $M_\infty = 0.70$; $M_{\ell,\max} = 1.30$.

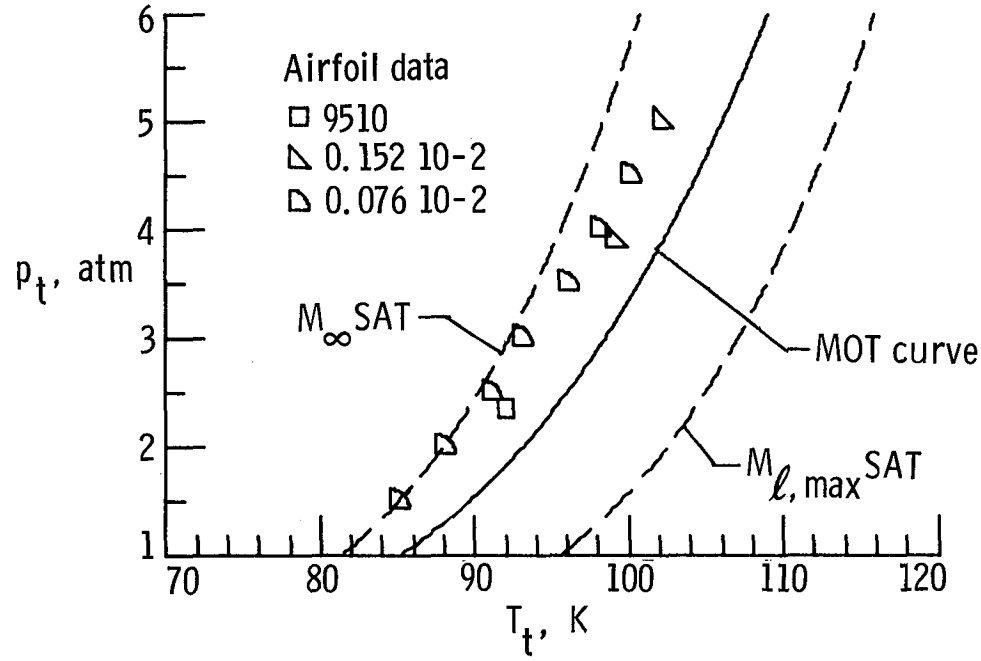

(d) $M_\infty = 0.65$; $M_{\ell,\max} = 1.40$.

Figure 24. Continued.

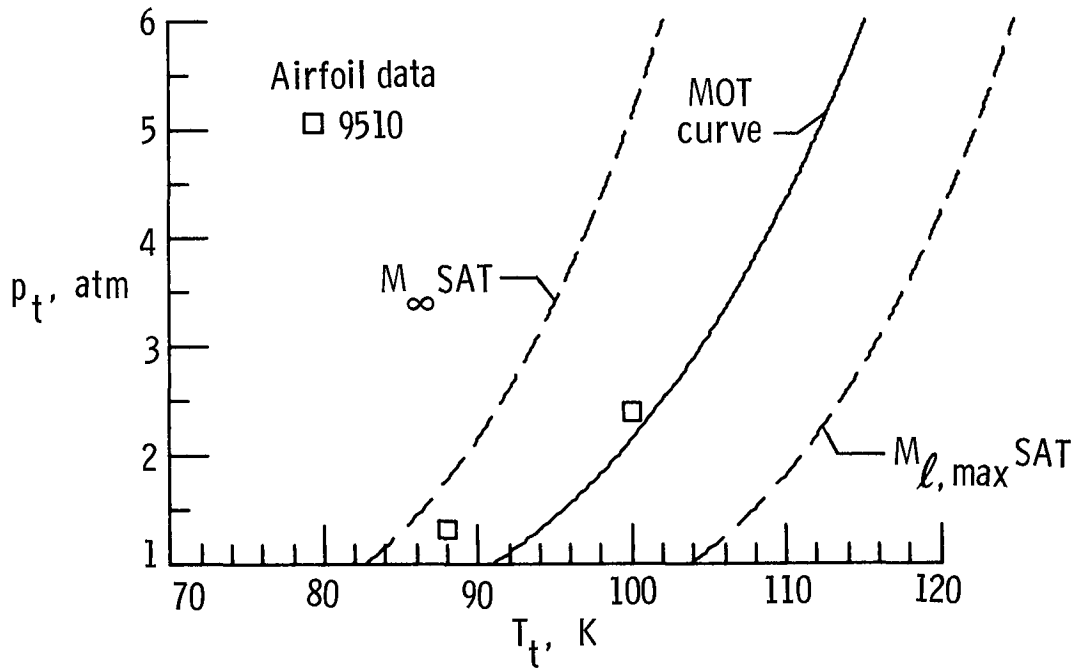

(e) $M_\infty = 0.75$; $M_{\ell,\max} = 1.70$.

Figure 24. Concluded.

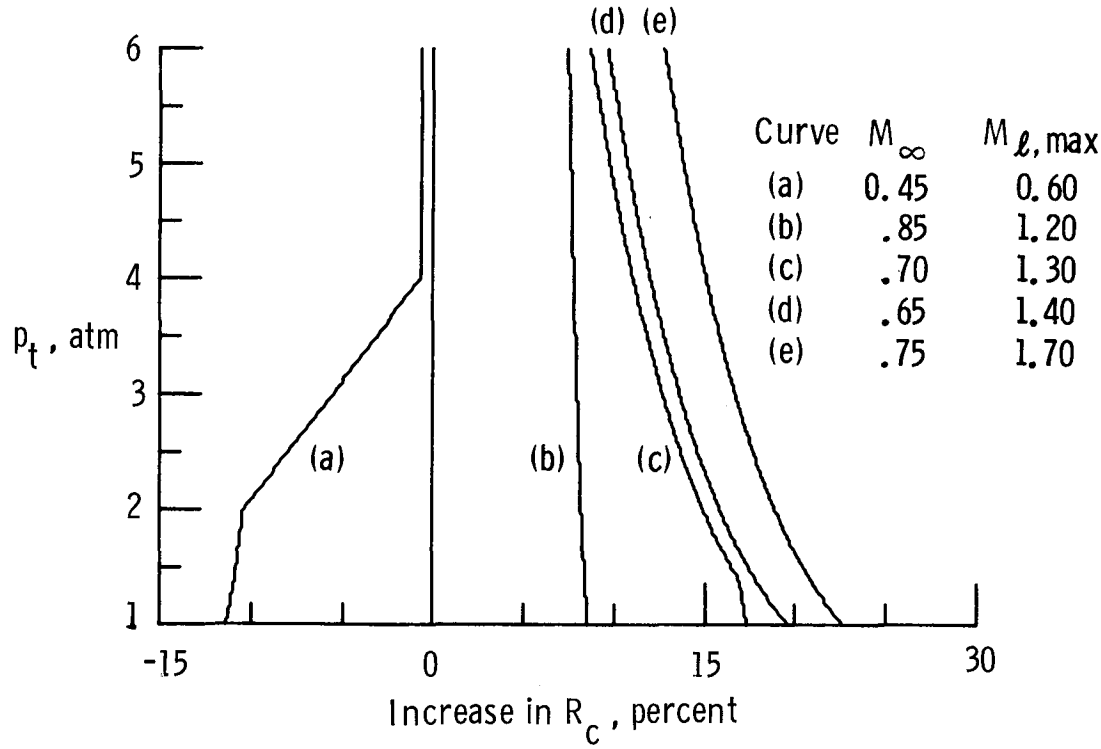

(a) Ideal-gas analysis.

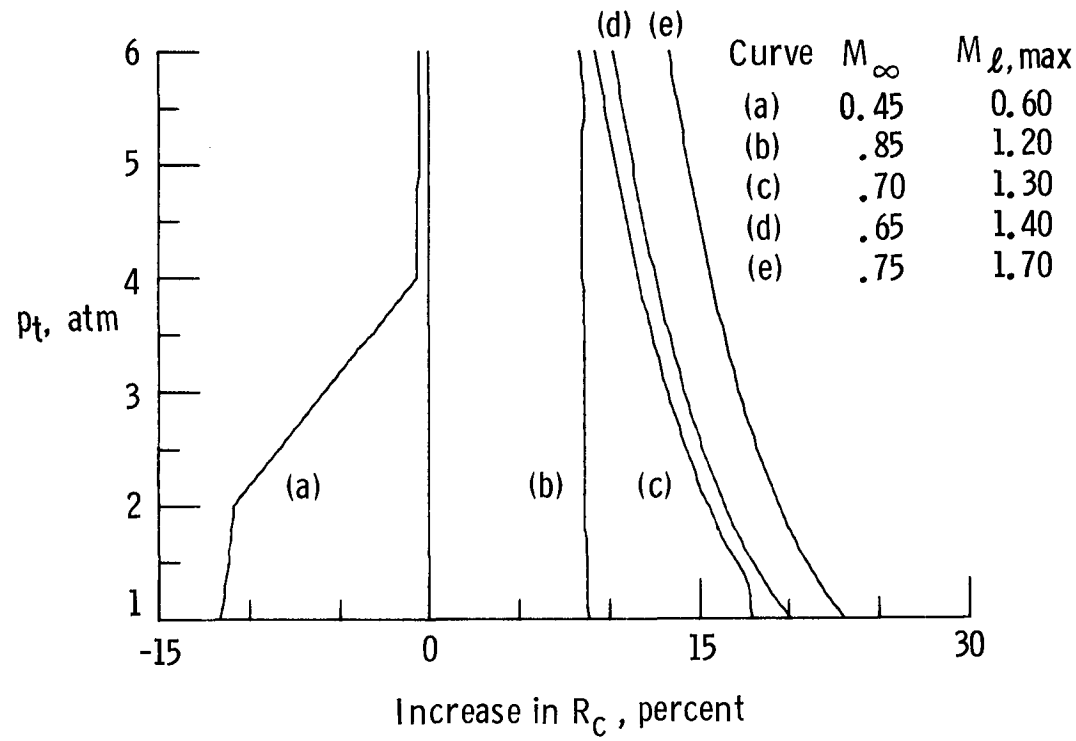

(b) Real-gas analysis.

Figure 25. Percent of increase in values of R_c calculated at MOT's compared with values of R_c calculated at temperatures corresponding to saturation at maximum local Mach numbers.

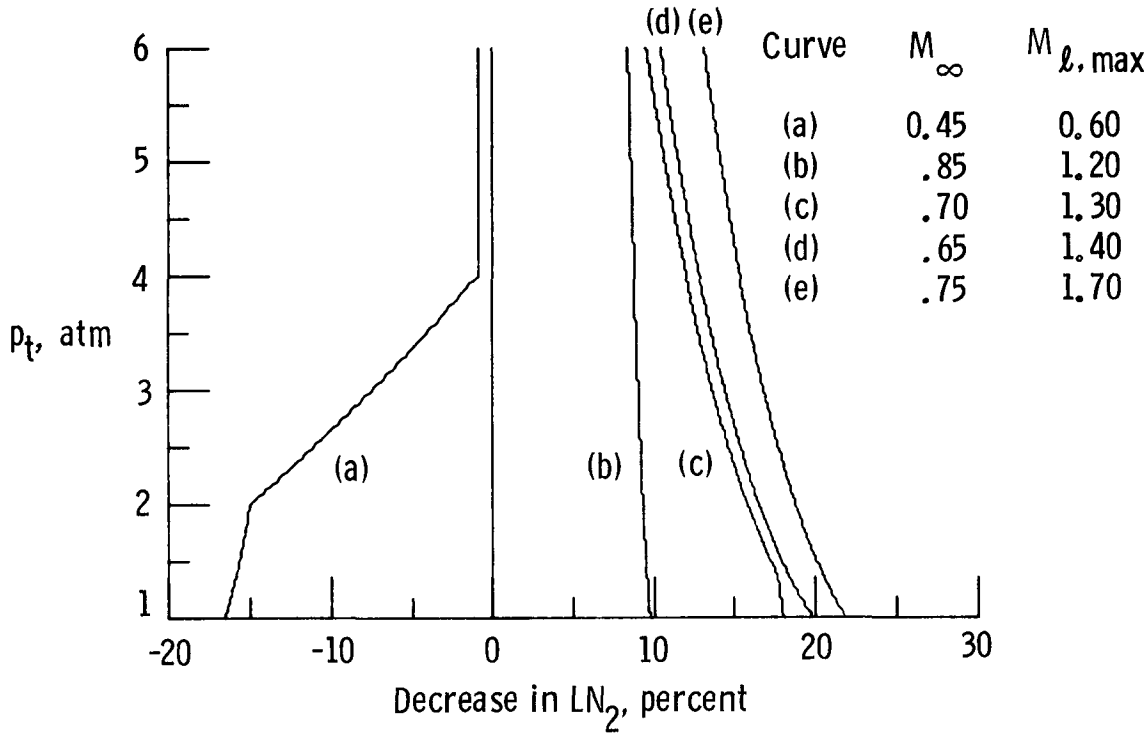

(a) Ideal-gas analysis.

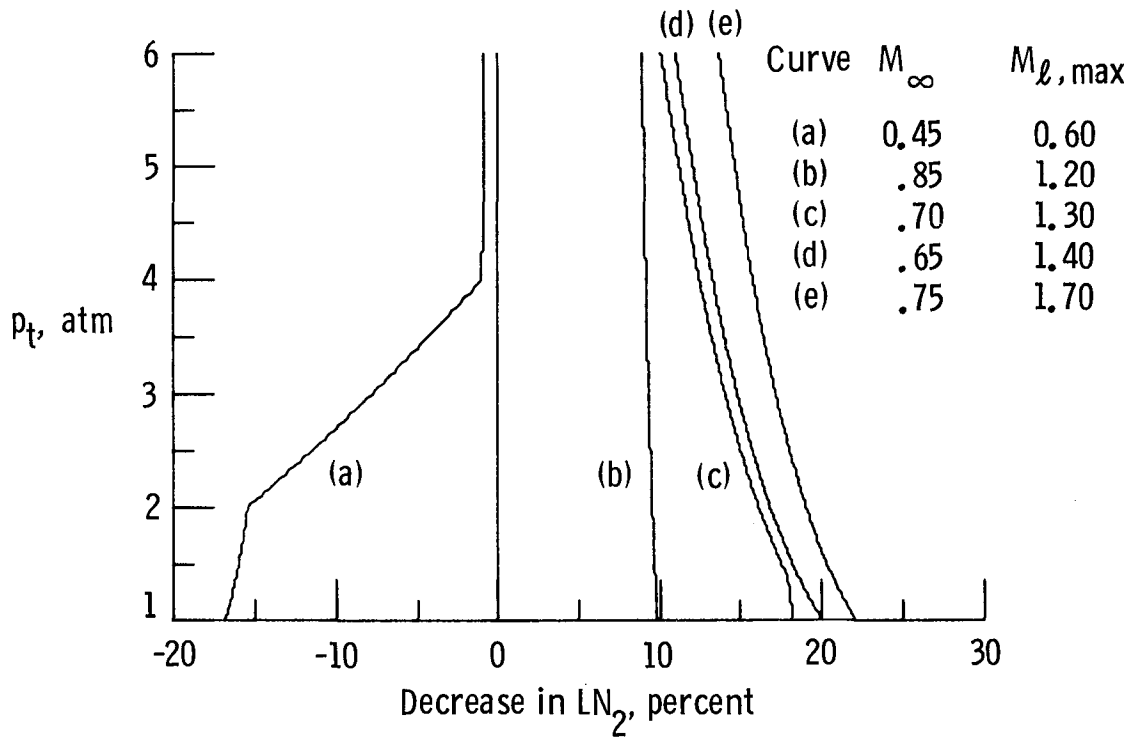

(b) Hybrid analysis.

Figure 26. Percent of decrease in values of LN_2 consumption calculated at MOT's compared with values of LN_2 calculated at temperatures corresponding to operation at the same unit Reynolds number, but at temperatures corresponding to saturation at maximum local Mach numbers.

1. Report No.	2. Government Accession No.	3. Recipient's Catalog No.
NASA TP-2509		

4. Title and Subtitle	5. Report Date
Studies of Condensation Effects on Airfoil Testing in the Langley 0.3-Meter Transonic Cryogenic Tunnel	January 1986
	6. Performing Organization Code: 505-31-23-07
7. Author(s): Robert M. Hall	8. Performing Organization Report No.: L-16021
9. Performing Organization Name and Address: NASA Langley Research Center, Hampton, VA 23665-5225	10. Work Unit No.
	11. Contract or Grant No.
12. Sponsoring Agency Name and Address: National Aeronautics and Space Administration, Washington, DC 20546-0001	13. Type of Report and Period Covered: Technical Paper
	14. Sponsoring Agency Code

15. Supplementary Notes

16. Abstract

The results of condensation studies in the Langley 0.3-Meter Transonic Cryogenic Tunnel (0.3-m TCT) utilizing the NACA 0012-64, NPL 9510, NACA 0012, NASA SC(3)-0712(B), and CAST 10-2/DOA 2 airfoils are summarized as follows: (1) both homogeneous nucleation and condensation on preexisting seed particles can occur, depending on the value of maximum local Mach number over the airfoil; (2) if poor atomization of the liquid nitrogen (LN_2) injected to cool the tunnel occurs, it is possible for unevaporated LN_2 droplets to cause changes in a pressure distribution at total temperatures greater than those corresponding to local saturation; (3) drag measurements do not appear to be as sensitive to the onset of condensation effects as the individual pressure orifices around the airfoils; (4) a theoretical analysis by Sivier correlates well with the present airfoil data; and (5) a simple procedure is presented to predict minimum operating temperatures in the 0.3-m TCT.

17. Key Words (Suggested by Authors(s)): Airfoil data; Nitrogen gas; Condensation; Cryogenic wind tunnels

18. Distribution Statement: Unclassified—Unlimited

Subject Category 34

19. Security Classif.(of this report)	20. Security Classif.(of this page)	21. No. of Pages	22. Price
Unclassified	Unclassified	32	A03

For sale by the National Technical Information Service, Springfield, Virginia 22161

NASA-Langley, 1986

National Aeronautics and
Space Administration
Code NIT-4

Washington, D.C.
20546-0001

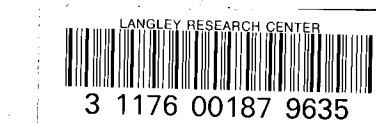

NASA